




Review

Magnetic Nanoparticle Systems for Nanomedicine—A Materials Science Perspective

Vlad Socoliuc ¹, Davide Peddis ^{2,3}, Viktor I. Petrenko ^{4,5,6}, Mikhail V. Avdeev ⁴, Daniela Susan-Resiga ^{1,7}, Tamas Szabó ⁸, Rodica Turcu ⁹, Etelka Tombácz ^{10,*} and Ladislau Vékás ^{1,*}

- ¹ Romanian Academy–Timisoara Branch, Center for Fundamental and Advanced Technical Research, Laboratory of Magnetic Fluids, Mihai Viteazu Ave. 24, 300223 Timisoara, Romania; vsocoliuc@gmail.com (V.S.); daniela.resiga@gmail.com (D.S.-R.)
 - ² Dipartimento di Chimica e Chimica Industriale, Università degli Studi di Genova, Via Dodecaneso 31, 16146 Genova, Italy; davide.peddis@gmail.com
 - ³ Istituto di Struttura della Materia-CNR, 00015 Monterotondo Scalo (RM), Italy
 - ⁴ Frank Laboratory of Neutron Physics, Joint Institute for Nuclear Research, Joliot-Curie Str. 6, 141980 Dubna, Russia; vip@nf.jinr.ru (V.I.P.); avd@nf.jinr.ru (M.V.A.)
 - ⁵ BCMaterials, Basque Centre for Materials, Applications and Nanostructures, UPV/EHU Science Park, 48940 Leioa, Spain
 - ⁶ IKERBASQUE, Basque Foundation for Science, 48013 Bilbao, Spain
 - ⁷ Faculty of Physics, West University of Timisoara, V. Parvan Ave. 4, 300223 Timisoara, Romania
 - ⁸ Department of Physical Chemistry and Material Science, University of Szeged, 6720 Szeged, Hungary; sztamás@chem.u-szeged.hu
 - ⁹ National Institute for Research and Development of Isotopic and Molecular Technologies (INCDTIM), Donat Str. 67-103, 400293 Cluj-Napoca, Romania; rodica.turcu14@gmail.com or rodica.turcu@itim-cj.ro
 - ¹⁰ Department of Food Engineering, Faculty of Engineering, University of Szeged, Moszkvai krt. 5-7, H-6725 Szeged, Hungary
- * Correspondence: tombacz@chem.u-szeged.hu (E.T.); vekas.ladislau@gmail.com or vekas@acad-tim.tm.edu.ro (L.V.)

Received: 10 November 2019; Accepted: 19 December 2019; Published: 2 January 2020



Abstract: Iron oxide nanoparticles are the basic components of the most promising magneto-responsive systems for nanomedicine, ranging from drug delivery and imaging to hyperthermia cancer treatment, as well as to rapid point-of-care diagnostic systems with magnetic nanoparticles. Advanced synthesis procedures of single- and multi-core iron-oxide nanoparticles with high magnetic moment and well-defined size and shape, being designed to simultaneously fulfill multiple biomedical functionalities, have been thoroughly evaluated. The review summarizes recent results in manufacturing novel magnetic nanoparticle systems, as well as the use of proper characterization methods that are relevant to the magneto-responsive nature, size range, surface chemistry, structuring behavior, and exploitation conditions of magnetic nanosystems. These refer to particle size, size distribution and aggregation characteristics, zeta potential/surface charge, surface coating, functionalization and catalytic activity, morphology (shape, surface area, surface topology, crystallinity), solubility and stability (e.g., solubility in biological fluids, stability on storage), as well as to DC and AC magnetic properties, particle agglomerates formation, and flow behavior under applied magnetic field (magnetorheology).

Keywords: magnetic nanoparticle systems; bio-ferrofluids; nanomedicine; single core; multi-core; synthesis; functional coating; physical-chemical properties; structural characterization; magnetorheology

1. Magnetism at Nanoscale and Bio-Ferrofluids—A Brief Introduction

Magnetic nanoparticle systems that are relevant for nanomedicine applications [1,2], such as biomedical imaging, magnetically targeted drug delivery, magneto-mechanical actuation of cell surface receptors, magnetic hyperthermia, triggered drug release, and biomarker/cell separation, have some particular features concerning composition, size, morphology, structure, and magnetic behavior, which highly motivated the synthesis, characterization, and post-synthesis application-specific modification of magnetic iron oxide and substituted ferrite nanoparticles [3–10]. These multi-functional magneto-responsive particles are highly promising in imaging and treating a lesion, simultaneously providing a theranostic approach [11–13]. Microscopic phenomena that are associated with the surface coordination environment, such as canted surface spins, intra- and interparticle interactions (dipolar or exchange, involving surface spins among different particles), and even increased surface anisotropy, which are relevant in improving magnetic field controlled driving and heating, as well as magnetic resonance imaging (MRI) detection, may affect the magnetic behavior of magnetic nanoparticle systems [14,15]. In the case ferrofluids designed for biomedical applications, the magnetic particles dispersed in aqueous carrier involve both single-core and multi-core iron oxide (mainly magnetite and maghemite) nanoparticles (IONPs), consequently *bio-ferrofluids* [16] widely extend the conventional domain of ferrofluids referring only to single core high colloidal stability magnetic nanofluids [17,18].

The interaction of a magnetic nanoparticle (MNP) with an external magnetic field [10] is governed by minimization of the dipole-field interaction energy achieved by the orientation of the particle's magnetic moment parallel to the applied magnetic field [3] and, in case of a non-uniform field, the interaction involves the translation of the particle in the direction of the field gradient, i.e., magnetophoresis [19]. The rotation of the magnetic moment of a particle that is suspended in a liquid carrier can occur either free with respect to the particle (Néel rotation) or together with the particle (Brown rotation) [4,20,21]. The orientation of MNP's magnetic moment in alternating current (AC) magnetic fields shows hysteresis, except for particular situations. The phenomenon of AC magnetic hysteresis is the basis of magnetic particle hyperthermia [21,22] and susceptometric granulometry of single and multicore MNPs [23]. In direct current (DC) magnetic fields, the magnetization of diluted single core particle dispersions follows the Langevin equation, which gives the theoretical framework for the magnetogranulometry of single core particles, due to the permanent magnetic moment of subdomain MNPs [24]. Depending on size, magnetic nanoparticles are subject of various contributions to their anisotropy energy [25–27], influencing the overall magnetic behaviour of the MNP system. The main forms of anisotropy specific to magnetic nanoparticles are summarized in what follows: (a) *Magnetocrystalline Anisotropy*: this property is related to the crystal symmetry and the arrangement of atoms in the crystal lattice. Magneto-crystalline anisotropy can show various symmetries, but uniaxial and cubic forms cover the majority of cases [28,29]. (b) *Magnetostatic anisotropy (shape anisotropy)*: this contribution is due to the presence of free magnetic poles on the surface creating a magnetic field inside the system (i.e., demagnetizing field) which is responsible for the magnetostatic energy. Subsequently, for a particle with finite magnetization and non-spherical shape, the magnetostatic energy will be larger for some orientations of the magnetic moments than for others. Thus, the shape determines the magnitude of magnetostatic energy and this type of anisotropy is often called as shape anisotropy [28,30,31]. (c) *Surface anisotropy*: Surface anisotropy, which increases with the increase in surface-to-volume ratio (i.e., a decrease in particle size), gives rise to the lower symmetry of surface atoms with respect to the atoms located within the particle [26,31]. Surface anisotropy is also strictly related to the chemical and/or physical interactions between surface atoms and other chemical species. The coating and functionalization of the nanoparticle surface can induce important modifications in its magnetic properties, referring to the so-called “magnetic dead layer” due to spin-canting [32–34].

Multicore particles have no permanent magnetic moment, provided that the constituent particles are small enough, such that the magnetic dipole-dipole interactions are negligible. The induced (resultant) magnetic moment of multicore particles is parallel to the external magnetic field and it follows the Langevin equation. The multicore particles show magnetic coercivity and remanence due

to dipole-dipole interactions if the constituent particles are large, i.e., the anisotropy energy overcomes the thermal energy. The induced magnetic moment of multicore particles at saturation is the sum of the constituent particles' magnetic moments [35]. Many applications of magnetic nanoparticles and nanocomposites in medicine rely on their ability to be manipulated while using magnetic fields. This ability depends on the effectiveness of the magnetophoretic force, being determined by the particle magnetic moment and the field gradient, to fix or to move the particles [19,36,37]. The magnetophoretic force exerted upon single core superparamagnetic nanoparticles is less effective due to their small diameter and magnetic moment implicitly, but, in the case of multicore composites, the resultant field induced magnetic moment is high enough in order to allow magnetic targeting already for moderate values of field intensity and gradient. Multi-core particles with relatively large overall sizes manifest strong magnetic response and, also, preserve the superparamagnetic behavior. Indeed, these multicore composites of sizes well above 20 nm show superparamagnetic properties at room temperature (300 K), while at very low temperature (~2 K) clusters of similar sizes would exhibit typical ferromagnetic hysteresis loops [38]. The particles' magnetic moment is more relevant than mass magnetization in order to assess the magnetic targeting/fixing applicability of magnetic particles [19,39,40].

In this review, we aim to focus on the latest trends in magnetic nanosystem research for nanomedicine applications, involving synthesis, structural, colloidal, magnetic and magnetorheological characterization, as well as demonstrating efficient progress and still existing weaknesses.

2. Designed Synthesis of the Magnetic Core

The preparation of superparamagnetic iron oxide nanoparticles (SPION) dispersions can be approached from two directions [41]: (i) from heterogeneous phases via dispersion (grinding and dispersing solid phase) of iron or iron oxides into aqueous solution and (ii) from homogeneous phases via condensation of precursors from either liquid or gaseous phase [42]. These have recently been called as the top down (mechanical attrition) and bottom up (chemical synthesis) methods of nanoparticle fabrication [43].

The bottom-up synthesis procedures [43–46], for example the coprecipitation of Fe(II) and Fe(III) salts, sol-gel processes, polyol methods, sonolysis [45], thermal decomposition, solvothermal reaction [47], hydrolytic and non-hydrolytic wet chemistry methods [3], liquid phase, polyols, thermal decomposition, microemulsion, and laser evaporation syntheses, biomineralization, [22], are considered to be the most effective ways of fabricating SPIONs. In a recent review [9], referring to the synthesis of shape-controlled magnetic iron oxide nanoparticles, it was emphasized that the nucleation and growth/agglomeration are the main stages in any colloidal or wet chemistry synthesis route. If monodisperse nanoparticles are aimed to be synthesized, the stages should be pulled apart in temperature and time, otherwise the polydisperse system and diverse particle morphology are obtained. For anisometric nanoparticles, like cubes, rods, disks, flowers, and many others, such as hollow spheres, worms, stars, or tetrapods, the growth is the crucial step and the specifically adsorbing ligands are responsible for the final morphology of nanoparticles. Uniform-sized nanoparticles from 3–4 up to 20 nm have been obtained through a seeded growth mechanism. The decomposition of iron stearate at high temperature in the presence of different surfactants allows to synthesize mixed crystals of magnetite and maghemite with sizes between 4 and 28 nm [48]. The synthesis parameters (precursors, additives, and their ratio) and experimental conditions (reaction time, temperature) were changed, and monodisperse, single core (this term was not used in the paper) crystals with different classes of size (e.g., 7–8, 10–11 nm) were made.

The thermal decomposition of organic precursors takes place in the presence of surfactant stabilizers. Nucleation events for the formation of the nanocrystals are controlled and, thus, the size and the use of surfactants allow for monodispersity. In this process, surfactant stabilized hydrophobic particles form that needs further treatments to transfer them into aqueous media. The latter can be achieved by using surfactants (e.g., Na-oleate), forming an oppositely oriented second layer due to hydrophobic interaction with the alkyl chains of first layer chemisorbed on the surface of IONPs [49]. The long-term stability of aqueous magnetic colloids under the effect of magnetic field in biorelevant

media has not been evidenced yet [17]. If oleic acid is used in the synthesis, the double bonds of chemisorbed oleate can be oxidized by strong oxidant (e.g., KMnO_4 under acidic or alkaline conditions). Azelaic acid forms in an oxidation reaction on the IONPs' surface, and the carboxylated product has good dispersibility in aqueous media [50]. The surfactants with hydrophobic alkyl chains can be replaced by hydrophilic molecules having functional groups (e.g., carboxylic acid, phosphonic acid, aromatic molecules with OH groups in ortho position) that have a higher affinity to $\equiv\text{Fe-OH}$ sites on IONPs' surface in a ligand-exchange process often used lately [51].

While keeping the superparamagnetic behavior, the synthesis of *multicore* particles proved to be a promising solution for magnetics based imaging, therapeutics, and sensing to improve the manifold magnetic response of particles [40,52–56]. Magnetic nanoparticle clusters embedded in a polymer shell, to sum the magnetic moments of each nanoparticle, were made applying in situ coprecipitation by using gels as microreactors [57,58], and also by strongly polar solvent induced destabilization of a ferrofluid [59]. The miniemulsion technique is also well-established to control clusterization of magnetic nanoparticles [60]. The densely packed magnetic clusters are encapsulated in a polymer shell [61,62]. High magnetization spherical particles in thermoresponsive polymer shell were produced in a ferrofluid miniemulsion procedure [63,64]. Hydrophobic oleic acid coated SPIONs of a light organic carrier (hexane, toluene, tetrahydrofurane) based ferrofluid may also be incorporated into chitosan amphiphile nanoparticles by the ultrasonic emulsification procedure and evaporation of the volatile carrier [65]. The magnetic behavior of nanoparticle assemblies is strongly dependent on interparticle interactions, in particular on dipole-dipole interactions and exchange coupling between surface atoms, with the size and molecular coating of magnetic nanoparticles controlling the resulting arrangements [66].

Various magneto-responsive nanocomposite particles with adjustable properties (e.g., size, magnetic moment, surface charge, morphology, shell thickness) were synthesized during the last period of time. Figure 1 collects some of these multi-core particles to illustrate the results in the design and manufacture of these magnetic carriers that have to respond to requirements of colloidal stability in aqueous dispersion media, as well as of achievable values of magnetic field strength and gradient. It is essential to ensure high values of the magnetic moment, which is one of the most important requirements, for successful applications in biomedicine of functionalized nanocomposite carriers, in particular in magnetic targeting [19,67,68]. In this respect there are different approaches to distribute a certain amount of magnetic nanoparticles, such as onto the surface of a non-magnetic core [69], or on layered silicate (e.g., montmorillonite) support with high surface area [70], enclosed in a thin vesicle bilayer [71], or close packed to form a magnetic core, the magnetic core-organic shell nanocomposites being favored by their high magnetic response [72]. MNP clusters that are prepared from aqueous [73] and organic [74] ferrofluids can be used to obtain magnetoliposomes [75] with high magnetic response and MRI contrast for in vivo drug and gene delivery into cancer cells. IONPs and anticancer drugs were enclosed into nanocapsules that were designed to be responsive to remote radio frequency (RF) field for ON-OFF switchable drug release [76]. Ferrofluids, as primary materials, provide hydrophobic IONPs to be encapsulated together with camptothecin anticancer drug into PPO (polypropylene oxide) block of Pluronic vesicles. The developed continuous manufacturing procedure is scalable and it provides multi-core theranostic drug delivery vehicles [77].

The usually spherical morphology resulting in oil (ferrofluid)-in-water miniemulsion procedure is modified when the hydrophobic oleic acid coating of MNPs is incomplete and the hydrophobic character of particles significantly reduces. As a consequence, the MNPs accumulate at the ferrofluid drop-water interface, resulting in *strongly non-spherical shape* nanocomposite particles [39]. Magnetic field guided evaporation of ferrofluid droplets [78,79], making use of specific Rosensweig instabilities and tuning the concentration of ferrofluid, allows for preparing various shaped nanocomposites (so-called “supraparticles”) and also preserving superparamagnetic behavior. The high evaporation rate organic ferrofluids having oleic acid monolayer coated magnetite NPs were used to fabricate magnetoactive *fibrous nanocomposites* and multi-responsive co-networks [80,81], which exhibit promising characteristics for magnetothermally or pH triggered drug delivery.

More recently *nanoflower type composites* came into the play [82], whose formation is due to exchange interactions between the cores favoring cooperative behavior and a crystal continuity at the core interfaces. The magnetic nanoflowers manifest enhanced susceptibility while maintaining superparamagnetic behavior; their structure (e.g., the contact between cores within a particle, having a strong impact on the collective magnetic properties [83]) critically depends on the synthesis process. Two routes of the latter can be differentiated: the polyol method and thermal decomposition. For example, the 1:2 mixture of Fe(II) and Fe(III) salts was hydrolyzed in organic solvent mixture (diethylene glycol and N-methyldiethanolamine) at high temperature; the clustering and coalescence of seeds took place during the longer period [84]. In this single step process, a big mixture of coalesced flower-like maghemite nanoparticles formed, which was fractionated by increasing salt content of aqueous system at low pH, taking advantage of electrostatic colloidal stability. Figure 2 shows the nanoflowers formed in the one pot synthesis and two fractions selected as examples to distinguish the single and multicore IONPs. Different routes based on the partial oxidation of Fe(OH)₂, polyol-mediated synthesis, or the reduction of iron acetylacetonate were used to obtain multicore iron oxide nanoflowers in the size range 25–100 nm [82]. The nanoparticles were either stabilized with well-known agents, such as dextran and citric acid, or, as an alternative, IONPs were embedded in polystyrene to ensure long-term colloidal stability. The first steps toward the standardization of the synthesis and characterization of nanoflowers have been attempted. By now, better quality of magnetite nanoflowers can be also synthesized by thermal decomposition in organic media [25].

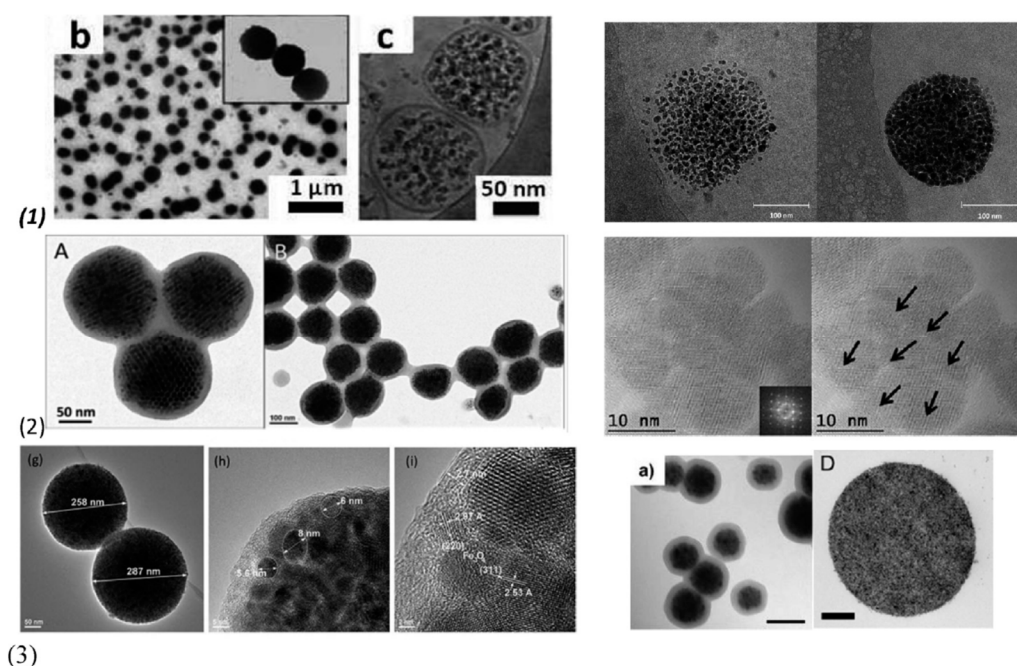


Figure 1. Magnetic multi-core particles obtained by different synthesis procedures: (1) *encapsulation of magnetic nanoparticles (MNPs) into liposomes, polymersome*: left—TEM (b) and cryo-TEM (c) micrographs of Ultra Magnetic Liposomes (UMLs) prepared by reverse phase evaporation process (REV) process. MNPs are trapped inside unilamellar vesicles (c) and dipole–dipole interaction can occur as exemplified by magnification (b) ([73]); right—Cryo-TEM image showing iron oxide nanoparticles incorporated in the polymersome membrane with 4.1% iron oxide (left), and 17.4% iron oxide (right) ([77]). (2) *thermal decomposition*: left—TEM images of polymer encapsulated colloidal ordered assemblies (polymer-COA) at higher (A) and lower (B) resolution. The dark pattern (A) results from the ordering of the closed packed assemblies within the nanobeads, while the brighter gray ring is caused by the polymer shell (lower electron density) of around 20 nm thickness ([59]); right—High Resolution TEM of multi-core MNP showing the continuity of the crystal lattice at the grain interfaces. The Fourier transform of this

high resolution image (see inset) shows the monocrystalline fcc structure of the multi-core nanoparticles, oriented along the [001] zone axis ([84]). (3) *miniemulsion*: *left*—TEM images of magnetic microgel with magnetite nanoparticles cluster as a core coated with two layers of cross linked polymer shells poly-N-isopropylacrylamide-polyacrylic acid ([63]); *center*—TEM image of magnetic clusters encapsulated in a copolymer hydrogel poly(N-isopropylacrylamide-acrylic acid). Scale bar: 100 nm ([62]); *right*—TEM image of cross section of superparamagnetic microparticles produced with ferrofluid nanoparticle concentrations of 1 g/L using oil-in water emulsion-templated assembly ([39]). Reprinted with permission from Reference [41].

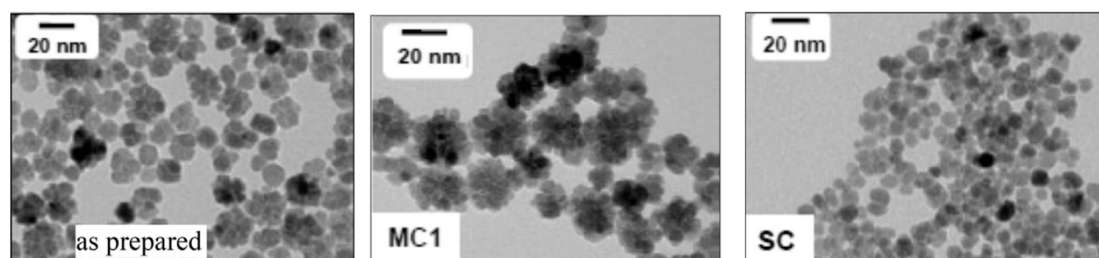


Figure 2. TEM images of the polydisperse mixture of iron oxide nanoparticles (IONPs) (as prepared left side) and its fractions containing multicore (MC1 middle) and single core (SC right side) nanoparticles. Reprinted with permission from Reference [84].

3. Magnetic Nanoparticles in Aqueous Carrier

3.1. Ferrofluids vs. Bioferrofluids

The main distinctive feature of ferrofluids among the larger class of magnetic colloids is their long-term colloidal stability, even in strong and non-uniform magnetic fields specific to most of applications. In the carrier liquid, the overall particle interaction potential should be repulsive, i.e., the attractive van der Waals and magnetic forces have to be balanced by Coulombic, steric or other interactions, in order to keep particles apart from each other [17]. The stabilization of magnetic fluids impeding aggregate formation is more challenging for aqueous than for organic carriers. The necessary increase of magnetic particle concentration also involves an increase of the hydrodynamic volume fraction of surface coated particles determined by the stabilization procedure, electrostatic or electro-steric, which differentiate water-based ferrofluids, to attain high values of saturation magnetization. The steric stabilizing layer (usually a chemisorbed primary and a physisorbed secondary layer of surfactant molecules) has a much greater thickness than the electrostatic one, therefore the hydrodynamic volume fraction at the same magnetic volume fraction is much higher (approx. 7–8 times) for electro-steric (e.g., oleic acid double layer) than for electrostatic stabilized aqueous ferrofluids [85]. The significantly reduced interparticle distance produces colloidal stability issues that involve nanoparticle size and magnetic moment, dipolar interactions, excess surfactant, and agglomerate formation. Ferrofluids designed for biomedical applications—bio-ferrofluids [16]—involve beside single-core particles, a large fraction of multi-core magnetic nanoparticles coated with single or multiple biocompatible surface layers [41], to be discussed in what follows.

3.2. Surface Coating of Magnetic Cores

The surface coating of magnetic iron oxide nanoparticles (IONPs) is inevitable to protect iron leaching, to optimize long term and in-use colloidal stability, to ensure biocompatibility, and to provide specific sites to graft biological functions as well. Therefore, the coating of magnetic nanoparticles should be carefully designed.

The different synthesis methods commonly produce IONP particles that are coated with a protective shell. The preparation of naked IONPs is relatively rare in the literature, probably for the reason that the surface properties of naked IONPs definitely depend on pH and nanoparticles strongly aggregate at neutral pHs, as discussed above [86,87]. The colloidal stability of IONPs under biorelevant conditions,

e.g., in blood, at pH~7.4 in physiological salts and protein concentration is the minimum requirement for biomedical applications [71,88]. Therefore, the aggregation of IONPs has to be prevented by protective coating, which can be created either during or after their synthesis. In the literature, in situ coating, post-synthesis adsorption, or post-synthesis grafting are distinguished [68]. In the latter, the functional groups of brush-like polymer chains are anchored to the IONP's surface. Covalently bound molecules can more improve colloidal stability than adsorbed ones, as demonstrated, for example, in the work of Rinaldi and co-authors [89,90]. However, a great disadvantage of the former is the expensive purification process to remove impurities from organic synthesis to reduce the chemical hazard of the formulation. The multipoint adsorption of polyelectrolytes, especially natural polysaccharides, such as chondroitin-sulfate-A (CSA) bound chemically to $\equiv\text{Fe-OH}$ surface sites of IONPs, is suitable for fabricating biocompatible magnetic fluid (MF) and magneto-responsive nanocomposites [91–94]. Biopolymer coated magnetite nanoparticles fulfill all assumption of biomedical application, as shown in Figure 3.

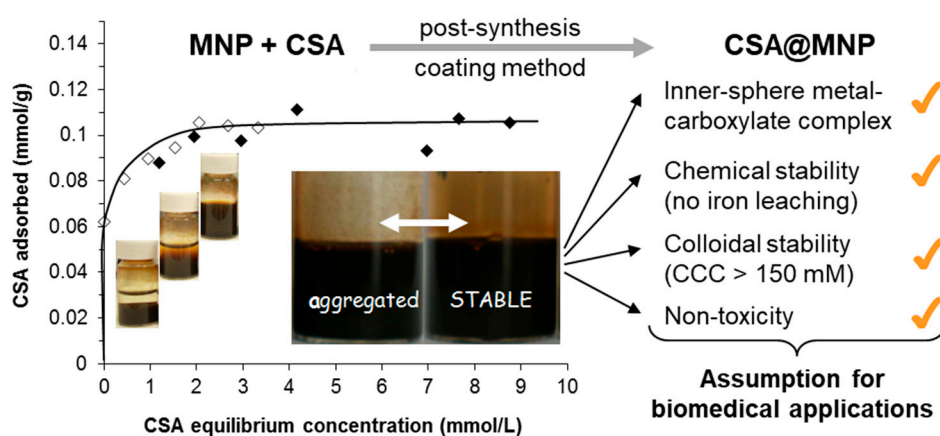


Figure 3. Adsorption isotherm of chondroitin-sulfate-A (CSA) on magnetite nanoparticles (MNP) at pH ~6.3 in aqueous NaCl solution (left side). With increasing CSA concentration, the colloidal state of samples changes characteristically from aggregated to stable, as seen in the vials. The inserted larger photos clearly show the difference between the well stabilized and aggregated magnetic fluids (the amount of CSA is expressed through the number of repeating units in mmol.) Some assumptions of biomedical application are listed in the right side of figure. Reprinted from Reference [94] under the terms of CC by 4.0.

In the literature, the biomedical use of citric acid stabilized IONPs is favored (e.g., the famous VSOP-C184 product) in [45,95,96] or of the multi-core samples in [97]). However, the citrated IONPs coagulate, even at low salt concentration and, moreover, their iron leaching is very high because citric acid has a reducing effect, and it forms complexes with the surface Fe ions [98]; the dissolved iron ions may cause oxidative stress besides the danger of particle aggregation in vivo. Amstad and coworkers [71] reported a similar iron dissolution effect of catechol derivatives (e.g., mimosine) grafted to Fe_3O_4 surfaces, causing the gradual dissolution of Fe_3O_4 nanoparticles through complexation. The other key point is the formation of protein corona of MNPs in biological fluids [99]. Up to now, the coating IONPs with hydrophilic agents is the most widely accepted method for overcoming this problem. Polyethylene oxides or glycols (PEG) and carbohydrates like dextran [3,71] or carbohydrate derivatives (such as mannose, ribose, and rhamnose) [84,100] are the most common of many coating agents, which are chemically bound to the $\equiv\text{Fe-OH}$ surface sites or by multiple H-bonds, and make IONPs super hydrophilic, inhibiting the adsorption of proteins. However, the formation of protein corona on MNPs covered with dextran and its derivatives has been perceived [101]. Other types of PEG coating on IONPs (grafting with poly(ethylene glycol)-silane [90] or in situ forming in the poly(ethylene glycol) and poly(ethylene imine) mixture [102]), i.e., the PEGylation can generally improve the drug delivery, enhance the drug accumulation, and might improve the blood-brain barrier transport of

IONPs [68]. A new design of PEGylated coating (P(PEGMA-co-AA)@MNPs) provides a non-fouling outer surface that helps the nanoparticles to remain “invisible” for the phagocytic mechanisms, while its free carboxylate moieties can be exploited for grafting specific biologically active molecules or proteins for theranostic applications [103].

Using the synthesis procedure of carboxylic (lauric, myristic or oleic) acid stabilized aqueous ferrofluids [49,104], bovine serum albumin (BSA) coating was applied to rise the colloidal stability of lauric acid-coated IONPs in biological media [105]. The coating greatly reduced the toxicity of nanoparticles and enhanced therapeutic potential of mitoxantrone drug-loaded system. Further cross-linking of BSA coating was performed in order to improve colloidal stability [106], and monoclonal antibodies were covalently bound to BSA coated IONPs promising MRI contrast agents for glioma visualization in brain.

Nanoparticles interact with biological entities in a biological environment, and nano-bio interfaces form [107]. Only the particle surface can be modified to improve in vivo biocompatibility of nanoparticles. Seeing this issue, the size, the sign, and magnitude of surface charge (as manifested in the measurable zeta potential) and dispersibility in aqueous media (hydrophilic/hydrophobic feature) are the main options for change. Experiments have already shown that positively charged particles are probably more toxic than the larger hydrophobic ones clearing rapidly in the reticuloendothelial (RES) system. In biological systems, medium-sized particles with a neutral or weakly negatively charged surface generally tend to promote enhanced permeation and retention (EPR) [107].

A new generation of coating agents P(PEGMA-co-AA), which combine charged functional groups (i.e., carboxyl groups that are capable of anchoring both nanoparticles and bioactive molecules) and superhydrophilic uncharged segments (i.e., PEG chains in comb-like arrangement) has been reported last year [103]. In a post-coating process, these multifunctional molecules are able to spontaneously bind to MNPs' surface sites $\equiv\text{Fe-OH}$; stabilize the particles electrostatically via the carboxylate moieties and sterically via the PEG moieties; provide high protein repellency via the structured PEG layer; and, anchor bioactive molecules via chemical bond formation with the free carboxylate groups. The electrosteric (i.e., combined electrostatic and steric) stabilization is efficient down to pH 4 and it tolerates saline media.

In biomedical applications, an optimized coating on SPION surface is required, via which IONPs can interact with different biological entities (proteins, cell membranes, etc.). Only the coating on the engineered NPs can be freely varied at the nanobio interface. The core of nanoparticles has almost all of the desired properties, such as chemical composition, shape and curvature, porosity and surface crystallinity, heterogeneity, and roughness, as listed by Nel and coworkers [107]. The coating layer of core-shell nanosystems provides optimal hydrophobicity/hydrophilicity in a given medium and active sites for anchoring biofunctions. In the same article, the other quantifiable properties of NPs' interactions (dissolution, hydration, zeta potential, aggregation/dispersion, etc.), which are crucially influenced by the ionic strength, pH, temperature, and the presence of large organic molecules (e.g., proteins), or specifically adsorbing molecules or ions (e.g., detergents generally or phosphate ions) of the suspending media, are separately discussed. The composition and structure of interfacial layer on coated NPs, as well as its changes on the nanoscale, definitely affect the microscale and more the macroscale behavior of engineered nanoparticles. The quality of coating interrelates with colloidal stability under biorelevant conditions, as described in [108]. Sedimentation, freezing, and hemocompatibility tests (smears) are recommended for the qualification of good and bad SPION manufacturing for intravenous administration. Besides the colloidal stability of nanosystems, coatings also largely affect the functionality and biological fate of IONPs. Several different functions of NPs' coating can be identified, namely: (i) colloidal stabilization under physiological conditions (protecting against aggregation at biological pHs and salty medium), (ii) inhibiting the corrosion and oxidation of magnetic core (passivation reducing the iron leakage), (iii) hindering non-specific protein adsorption in biological milieu, (iv) providing reactive groups for anchoring drugs and targeting molecules, and (v) controlling nano-bio interfacial interactions (bio/hemocompatibility, reticuloendothelial system

(RES) uptake, blood circulation time, IONP's internalization efficiency, toxicity, targeting efficiency, in vivo fate, etc., as discussed in detail [3,41,68,71,107]). These functions of coating largely overlap with the general concerns of EMA (European Medicines Agency) [109] that should be considered in the development of nanomedicine products.

3.3. Stabilization Mechanisms

The dispersed nanoparticles move freely (thermal motion) in the carrier medium. The colloidal stability of dispersion is the question, whether nanoparticles can retain their separateness during collisions; i.e., whether the particle-particle interactions that are controlled by the frequency and efficiency of collision result in aggregate or not. The latter depends on the extent of attractive and repulsive contributions to the total interaction. The classical DLVO theory of colloidal stability describes the attractive (van der Waals) and repulsive (electrostatic) forces. In addition to these, the hydration, the hydrophobic interactions, and the steric hindrance should be also assessed [110,111]. In the case of magnetic particles, besides the short range exchange interaction especially relevant to formation of multi-core particles, such as nanoflowers [83], the magnetic dipole attraction having a fundamental effect on the collective magnetic properties must also be taken into account [112] to obtain reasonable theoretical stability predictions [90]. In these papers particle aggregation is used as a generic term for coagulation and flocculation independently of the inner structure of aggregates and the reversibility of their formation. Another term, agglomeration, has appeared in the relevant literature, with the same or different meanings as aggregation. Gutiérrez and coworkers [83] reviewed the aggregation of magnetic iron oxide colloids and definitely stated that “nanoparticles tend to form assemblies, either aggregates, if the union is permanent, or agglomerates, if it is reversible”, recalling a bit industrial terminology or that used in nanotechnology nowadays. However, there are certain inconsistencies with the classical colloid nomenclature (e.g., in refs. [110,111]), where aggregation involves coagulation and flocculation giving rise to compact and loose structures, respectively. Their reversibility depends on the magnitude of mechanical force against they should exist. For example, coagulum, the aggregate that forms in the coagulation process, is irreversible against thermal motion; however, it disintegrates when subjected to stronger shaking, stirring, or even mild ultrasonication, and, after this, coagulation restarts at rest, so its formation is reversible [111].

In [113], it was emphasized that nanomaterials should be characterized in the relevant medium, and not simply in water, especially in what concerns aggregation (agglomeration) processes. Referring to coagulation kinetics, IONPs' colloidal stability should be acceptable under biorelevant conditions, i.e., at biological pH values, in the presence of salt and proteins, and also in cell culture media. In classical colloid science, coagulation kinetics can correctly characterize colloidal stability, also allowing for predicting the stability of SPIONs' products both on storage and in use. However, the measurements require advanced instrumentation and a lot of time, thus a simpler method would be needed to test SPION preparations [108]. Particle aggregation tests (size evolution, filtration, sedimentation, etc.) under arbitrary conditions are often used [71]. Coagulation kinetics is useful for testing the salt tolerance of IONPs and predicting their resistance against aggregation under physiological condition [87]. A straightforward route of physicochemical (iron dissolution) and colloidal (pH-dependent charging and particle size, salt tolerance from coagulation kinetics) measurements was suggested for assessing the eligibility of IONPs for in vitro and in vivo tests [98].

4. Physical-Chemical Characterization

4.1. Chemical Composition of Magnetic Nanoparticles

X-ray Photoelectron Spectroscopy (XPS) is a very sensitive surface analysis method for the materials chemical composition. The method allows for the determination of the atomic concentrations, the chemical state of the emitting atoms (oxidation degree, valence states, chemical ligands, etc.). This information results from the areas delimited by the photoelectron peaks and from the chemical

shifts of the peaks with respect to the elemental state, as induced by the chemical surrounding of the atoms. The electrostatic interaction between the nucleus and the electrons determine the core binding energies of the electrons. The electrostatic shielding of the nuclear charge from all other electrons in the atom reduces this interaction. The removal or addition of electronic charge will alter the shielding: withdrawal of valence electron charge (oxidation) increase in binding energy; addition of valence electron charge decrease in binding energy. Chemical changes can be identified in the photoelectron spectra.

In the case of magnetic nanoparticles, surface properties strongly influence their magnetic performance and their behavior in biological media. The core-shell type magnetic nanoparticle systems consist of the magnetic core and a shell around the core, usually a biocompatible polymer and additionally molecules fulfilling the roles of anchors, spacers, and various functionalities. XPS provides information regarding the chemical composition of the coating layers and, on the other hand, allow for determining the oxidation state of the metal in the magnetic core [63,114–117]. XPS allows for determining the oxidation states of iron and to quantify Fe^{2+} and Fe^{3+} ions in iron oxide nanoparticles. These oxidation states of iron can be determined by Fe2p spectrum employing chemical shift and multiplet splitting and the characteristic satellites [85,118–122].

The organic coating layers of magnetic nanoparticles have major importance for biomedical applications of these nanomaterials. Coating layers ensures the chemical and colloidal stability of magnetic nanoparticles and allow for further functionalization [122–124]. Surface functionalization of magnetic nanoparticles for biomedical applications remains a major challenge. XPS is one of the most appropriate methods for the analysis of the functionalized organic coating of magnetic nanoparticles. The optimization of the required properties for applications requires understanding the nature of the interface between the magnetic core and the shell and the influence of the surface complex formation on the nanoparticle's magnetic properties.

Mazur and coworkers reported a good strategy for surface functionalization of magnetic nanoparticles allowing for the simultaneous attachment of dopamine anchors bearing azide, maleimide, and alkyne terminal groups [125] (Figure 4). This functionalization strategy of nanoparticles by using dopamine derivatives shells has the advantage that, besides the protection of the iron oxide core offering the possibility to integrate in a one-step reaction several reactive sites onto the nanoparticles, making these functionalized nanoparticles very promising for biomedical applications.

XPS allows for a detailed analysis of surface chemical composition of iron oxide nanoparticles before and after functionalization with dopamine derivatives (Figures 5 and 6).

The ratio $\text{Fe}/\text{O} = 0.73$ was calculated from XPS spectra, which is in-between that of Fe_3O_4 (0.75) and Fe_2O_3 (0.66). This fact and the peak position and satellite peaks in Fe2p spectrum indicate that the magnetic core contains Fe_3O_4 and Fe_2O_3 . The presence of dopamine derivatives shells on the magnetic core was evidenced in the high resolution spectra of N1s and C1s core level spectra. The deconvoluted N1s spectra of Fe_3O_4 that were coated with dopamine derivatives (Figure 6) evidence the characteristic groups of the organic shells. The calculated atomic ratio C/N is a good estimation for the success of the organic coating on magnetic nanoparticles. The XPS spectra and the calculated atomic concentrations for the elements C, O, N, and Fe evidence the coating of the magnetic nanoparticles with dopamine derivatives.

The coating layers largely influence the colloidal stability of magnetic nanoparticles under physiological conditions [3,68,71,107]. The protein corona's effect differs significantly, depending on the surface chemistry of the nanoparticles. The surface chemistry strongly influences the formation of protein corona and the cellular uptake of the nanoparticles. Differences in protein corona formation have been observed for magnetic nanoparticles coated by different organic layers [126,127]. Szekeres et al. undertook a comparative study of the effect of protein corona formation on the colloidal stability of magnetic nanoparticles coated by polyelectrolyte shells, citrate (CA@MNP), and poly(acrylic-co-maleic acid) (PAM@MNP) [128]. PAM coating of MNP ensures a better stability at higher human plasma concentrations as compared with CA coated MNP. XPS determined the chemical composition (atomic

concentrations), as well as the chemical state of the atoms at the surface magnetic nanoparticles CA@MNP and PAM@MNP. The relevant differences between the nanoparticles CA@MNP and PAM@MNP can be observed in the XPS spectra for C1s core levels (Figure 7). Both spectra of C1s contain the carboxylic groups and in the case of CA@MNP the C-OH group appears according to the characteristic coating shells.

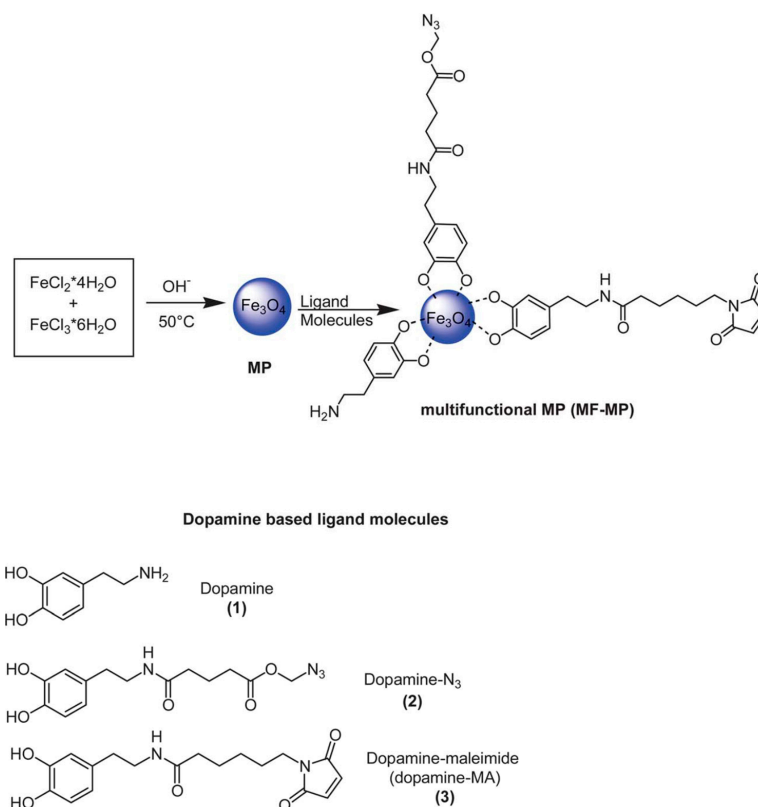


Figure 4. Schematic illustration of the formation of magnetic fluid-multifunctional magnetic nanoparticles (MF-MPs) based on the use of differently functionalized dopamine derivatives. Reprinted with permission from Reference [125].

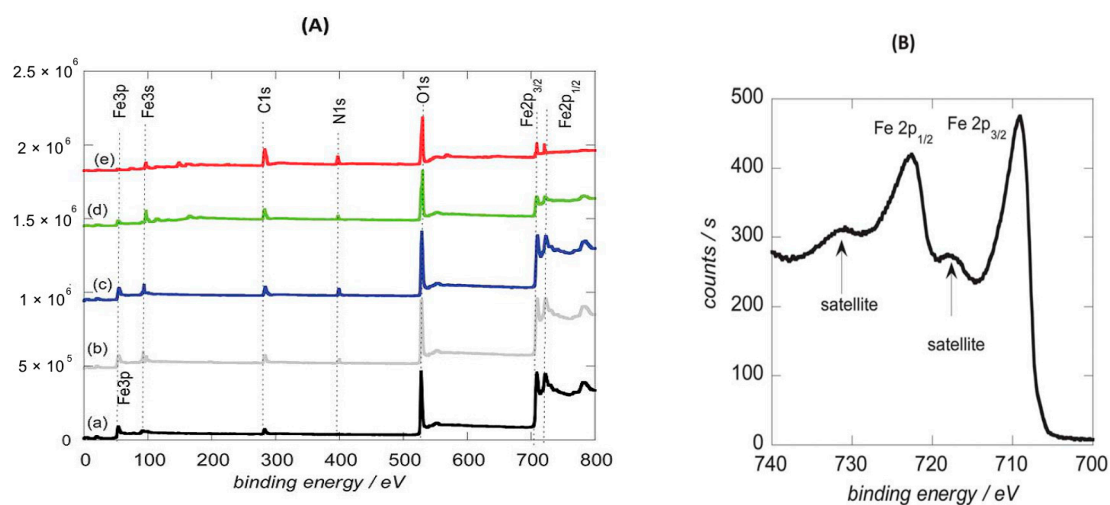


Figure 5. (A) X-ray Photoelectron Spectroscopy (XPS) survey spectra of as prepared magnetic particles before (a, black) and after modification with dopamine (b, grey), dopamine-N₃ (c, blue), dopamine-MA (d, green), and of MF-MP (e, red). (B) High resolution Fe2p spectrum of as-synthesized magnetic particles. Reprinted with permission from Reference [125].

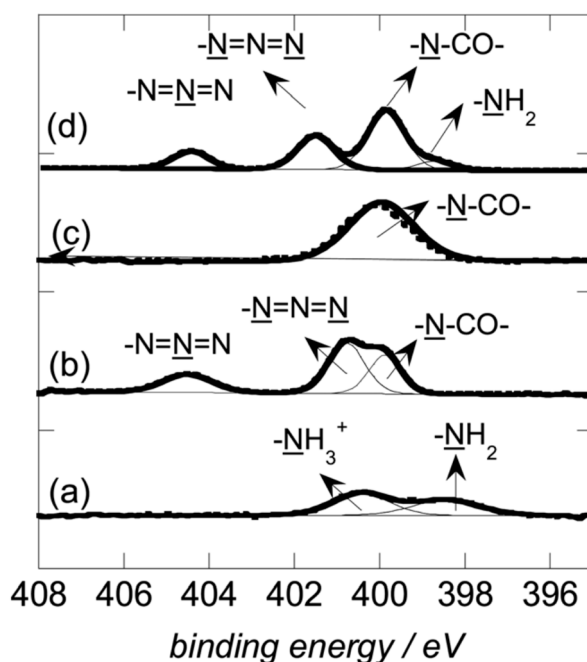


Figure 6. XPS N1s high resolution spectrum of magnetic particles modified with dopamine (a), dopamine-N3 (b), dopamine-MA (c), and MF-MPs (d). Reprinted with permission from Reference [125].

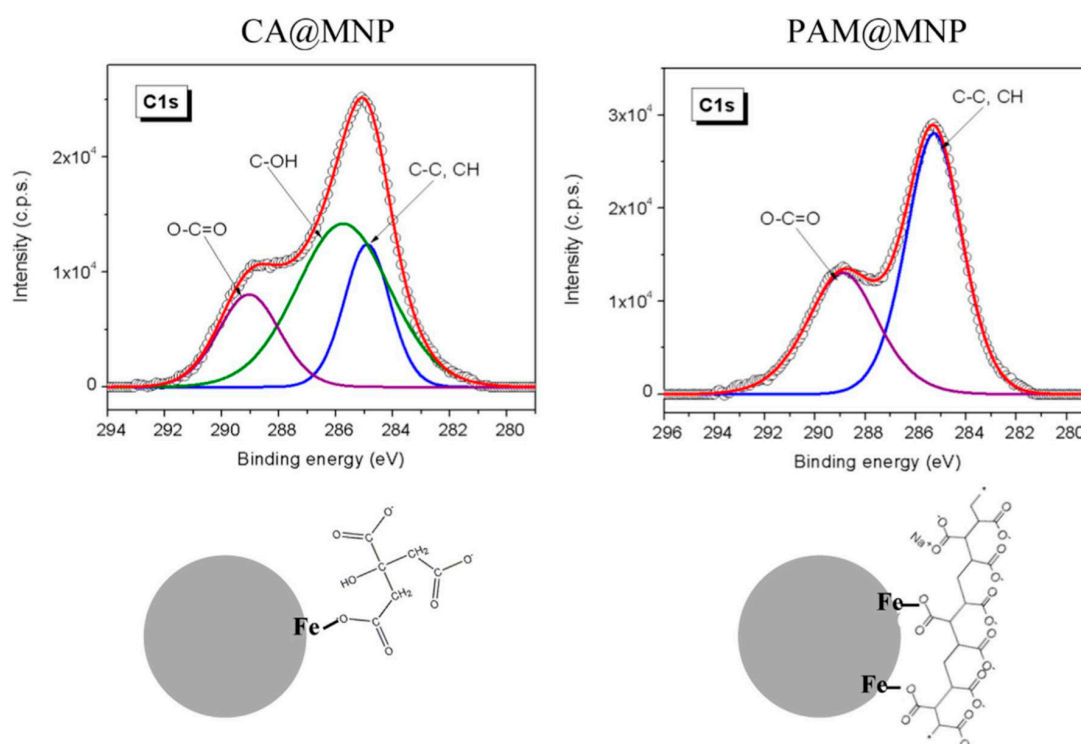


Figure 7. C1s spectra of the core-shell MNPs and the schemes of Fe–O–C(O)–R binding between MNP iron sites and organic carboxylates. Peak positions for CA and PAM coated MNPs: C–C, CH 284.91 and 285.27 eV; O–C=O 289.05 and 288.9 eV, respectively, and C–OH 285.75 eV for CA@MNP. Reprinted with permission from Reference [128].

4.2. Colloidal Stability. Zeta Potential and Hydrodynamic Size

The electrosteric (electrostatic+steric) stabilization has been shown to be quite effective; for example, polyelectrolyte (polyacrylic or polylactic acid, polyethylenimine, etc.) coating on IONPs

provides excellent stability [108]. However, outstanding salt tolerance can be achieved through hydrophilic polymer coating, such as dextran, a polysaccharide, which is used commonly in aqueous magnetic fluids [68,95,129]. Silica materials [130], organic molecules (e.g., carboxylates, phosphates, phosphonate, sulfates, amines, alcohols, thiols, etc. [68,88,95]) are often applied as coating agents to ensure colloidal stability. The functional groups of organic agents are mostly chemically bound to the reactive (both charged and uncharged) sites on IONPs' surface. For example, citrate through its OH and COOH groups are chemically linked to $\equiv\text{Fe}-\text{OH}$ sites in the citrated-electrostatic stabilized-magnetic fluids [98] or dopamine by two phenolic OH groups in the favored core-shell products [71,95]). The effect of surface coverage is hardly studied. IONP dispersions coagulate at a pH below PZC (point of zero charge), if polyacids, such as polyacrylic acid, are present in trace amounts, while their higher loading covers completely IONPs' surface and improves the stability and salt tolerance of colloidal iron oxide dispersions [68,131]. Macromolecules adsorb at multiple sites of surface, the so-called multi-site bonding makes the coating layer resistant against dilution and the purification of equilibrium medium easy [110,132].

To illustrate the significance of the stabilization mechanism applied-electrostatic or electrosteric-the zeta potentials and hydrodynamic sizes were measured for citrate and oleate stabilized aqueous ferrofluid samples and are given in Figure 8 to show the characteristic pH-dependence due to the different dissociation behaviors of the acidic groups on the coating molecules [85].

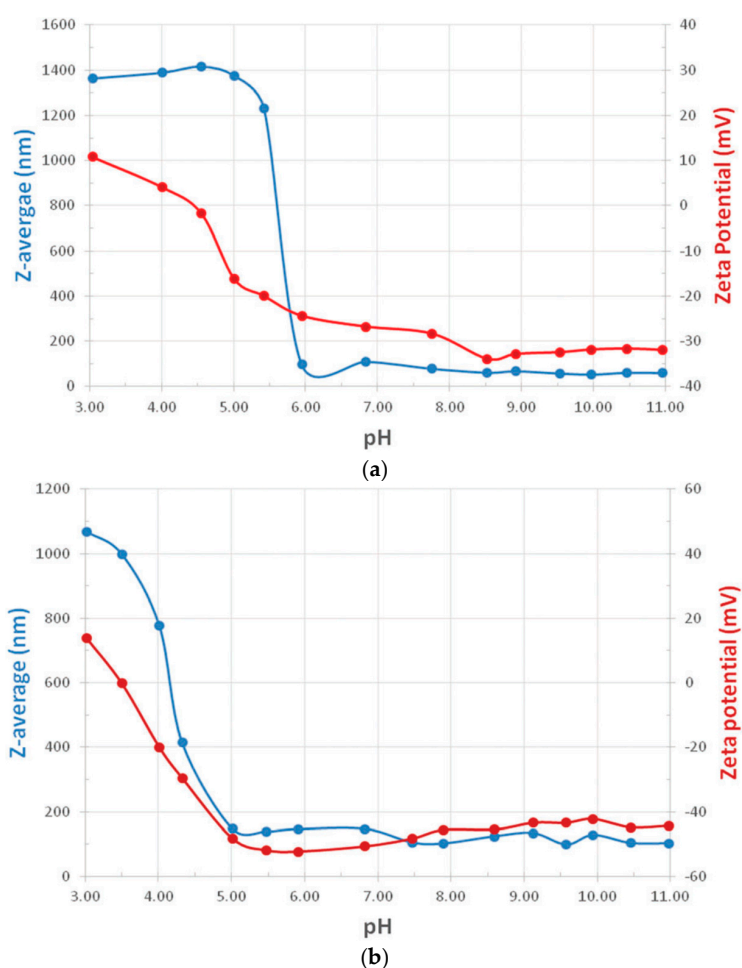


Figure 8. (a) pH dependence of the Z-average particle diameter (blue) and the zeta potential (red) for the citrated (MF/CA) sample. (b) pH dependence of the Z-average particle diameter (blue) and the zeta potential (red) for the oleic acid double layer stabilized (MF/OA) sample. Reprinted with permission from Reference [85].

The MF/CA sample loses colloidal stability below pH6 (Figure 8a) due to the difference in the charged state of citrated and oleic acid double layer coated MNPs, while the MF/OA ferrofluid below pH5 (Figure 8). This behavior is explained by the different dissociability values for citric acid ($pK_{a1} = 3.13$, $pK_{a2} = 4.76$, and $pK_{a3} = 6.40$) and oleic acid ($pK_a = 5.02$). Additionally, from Figure 8a,b, it follows that over a broad range of pH values, where both type of samples are stable, the citrate covered particles have a smaller Z-average diameter than the oleic acid covered nanoparticles.

4.3. Magnetic Properties

The magnetic field dependence of the magnetization, i.e., the magnetization curve, provides information regarding the magnetic properties of single and multicore magnetic nanoparticle systems. The magnetization of single and multicore magnetic nanoparticle systems is conditioned by the magnetic relaxation processes that are specific to the composition, dimension, morphology, etc., as well as external conditions, like temperature.

The direct current (DC) magnetometry is the most frequently used magnetic characterization method. The DC magnetization can be measured by means of vibrating sample magnetometry (VSM), alternative gradient magnetometry (AGM), and superconducting quantum interference device (SQUID). Important characteristics of the sample can be directly obtained from the magnetization curve: initial susceptibility (χ_i), saturation magnetization (M_s), coercive field (H_c), and remanent magnetization (M_r). In the case of superparamagnetic systems, the DC first magnetization curve can be used to determine the statistic of the nanoparticles' magnetic diameter by means of magnetogranulometry [133]. Figure 9 presents the DC magnetization curve and the theoretical fit [24] for a sample of dried magnetic microgels with magnetite nanoparticles [35]. The inset of Figure 9 shows the nanoparticle size distributions that were obtained from magnetogranulometry and TEM.

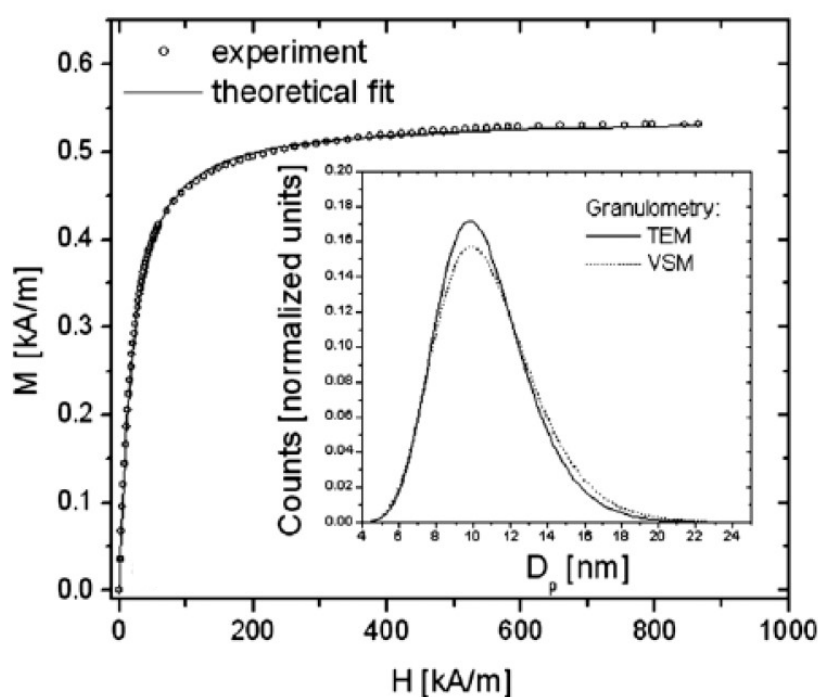


Figure 9. Direct current (DC) magnetization curve and the theoretical fit for a sample of dried magnetic microgels with magnetite nanoparticles. Reprinted with permission from Reference [35].

Several groups recently developed AC magnetometry [134,135] with the aim of determining the hysteresis loss in magnetic nanoparticles used in magnetic hyperthermia applications. The method is generally useful for characterizing the magnetic dynamic response of single and multicore magnetic nanoparticle systems at low and high frequencies in the range 1 kHz–1 MHz. Figure 10 presents

the frequency dependent dynamic response for 9 nm (Sample I—Figure 10a) and 21 nm (Sample II—Figure 10b) iron oxide nanoparticles, respectively [134]. The hysteretic loss is significantly larger in the bigger diameter nanoparticle sample.

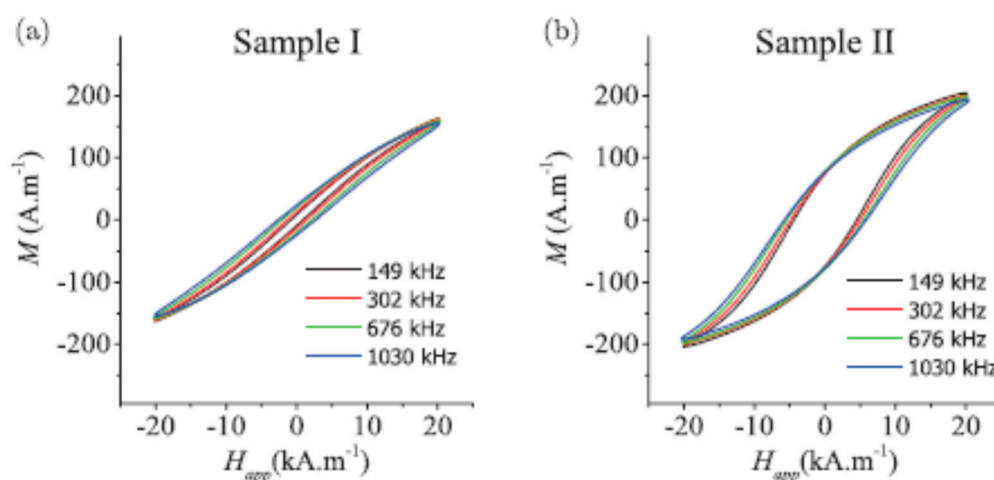


Figure 10. Dynamic hysteresis at different magnetic field frequencies for two iron oxide nanoparticle diameters: (a) Sample I 9 nm and (b) Sample II 21 nm. Reprinted with permission from Reference [134].

AC susceptometry measures the frequency dependence of the real and imaginary part of the magnetic susceptibility [133]. AC susceptometry is sensitive to the colloidal state of the magnetic nanoparticle dispersion, apart from being useful for the characterization of the relaxation mechanisms of the magnetic moment at the nanoscale. Figure 11a presents the frequency dependence of the normalized components of the complex susceptibility of a ferrofluid sample at different moments of the phase separation process [136]. Figure 11b shows the phase separation in a 10 mT DC field. Thus, it is shown the nontrivial influence of the magnetically induced phase separation on the complex susceptibility spectrum of ferrofluids.

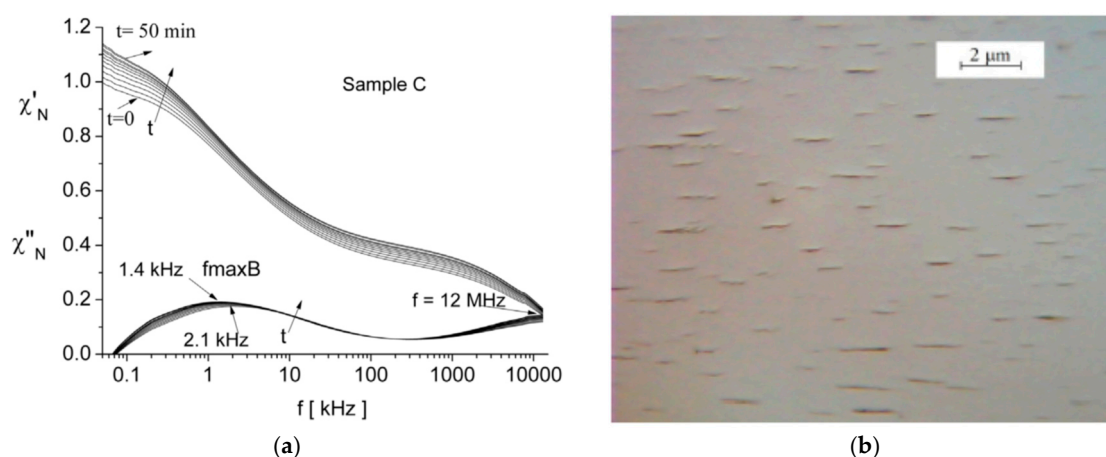


Figure 11. (a) Frequency dependence of the normalized components of the complex susceptibility of a ferrofluid sample and (b) optical microscopy image of magnetically induced phase separation. Reprinted with permission from Reference [136].

ZFC-FC measurements can characterize the superparamagnetic state of magnetic nanoparticles either isolated or in multi core environments [133]. The sample is cooled down from the superparamagnetic state to the lowest achievable temperature and the magnetization is measured while heating up the sample in an ~ 100 Oe applied field (ZFC) and afterwards the magnetization is measured while cooling the sample down again under the same applied field (FC).

4.4. Structural Characterization of Magnetic Colloids by Scattering Techniques

4.4.1. Neutron and X-ray Scattering

Scattering methods (neutron or X-rays) are powerful techniques for structural characterization at the nanoscale and contribute much to the development of nanomaterials. It is well known that the properties of the systems containing nanoparticles, such as liquid dispersions, are strongly related to the shape and size of the nanoparticle. Thus, systematic studies of these structural and morphological characteristics are required. Nowadays, small-angle scattering (SAS) and reflectometry are widely applied for nanostructure characterization in bulk and at interfaces, respectively. The main difference between neutron and X-ray scattering is the sensitivity to various chemical elements and their spatial distributions. The sensitivity to magnetic structures in the objects under study is an additional possibility for neutron scattering.

In the course of the SAS experiment, the widening of the neutron or X-ray beam that passed through the sample is analyzed in terms of the differential scattering cross-section per sample volume as a function of scattering vector module. Such dependence is quite sensitive to structural features of the studied systems at the scale interval of 1–300 nm [137], which makes SAS an ideal tool for the structural characterization of ferrofluids [138–140], since the size of particles in them are mostly in this dimensional range. Specific techniques, such as contrast variation and scattering of polarized neutrons, are used in small-angle neutron scattering investigations. From small-angle neutron (SANS) and X-ray (SAXS) scattering, it is possible to derive information regarding particle structure (size, polydispersity, stabilizing shell thickness, composition of particle's core and shell, solvent rate penetration in surfactant layer, structure of possible micelles in solutions), magnetic structure (magnetic size and composition), particle interaction (interparticle potential, magnetic moment correlation, phase separation), and cluster formation (developed aggregation and chain formation). The main task of the SAS experiment is to find out the distribution of scattering length density (SLD), which is defined as a specific sum of the coherent scattering lengths of atoms in a sufficiently small volume and it is usually represented in units of 10^{10} cm^{-2} .

Studying the reflectivity of the radiation (neutrons or X-rays) from planar surfaces is the basic idea of the reflectometry method [141]. The classical analysis of specular reflectivity allows one to determine an SLD profile (thickness, density, and roughness of each layer at interfaces) for the studied object in a direction perpendicular to the interface for a thickness up to hundreds nm with a resolution of 1 nm. The analysis of off-specular (diffuse) neutron scattering makes it possible to characterize lateral correlations on the surface and interlayer boundaries. It should be noted that the active use of the reflectometry method for investigations of ferrofluid structures at interfaces was started about a decade ago (e.g., [142]).

The structural features of several kinds of aqueous magnetic fluids [143–146], as well as surfactant/polymer solutions [147–149], which are used for magnetic nanoparticle stabilization in water, were investigated in detail by SANS (Figures 12 and 13). Additionally, magnetic nanoparticles with bio-macromolecules were successfully studied by SANS and SAXS [150,151] (Figure 14). Thus, investigations of magnetic fluid stability at various amounts of surfactants and aggregation of MNPs were undertaken by SAS for ferrofluids based on non-polar and polar (aqueous) carriers. For water-based ferrofluids with sterical/charge stabilization (double-layer coating of magnetite nanoparticles by sodium oleate (SO) or dodecylbenzene sulfonic acid (DBSA)), the fraction of micelles of formed by non-adsorbed surfactant molecules was found by SANS (Figure 12). It was shown that the different rate of surfactant adsorption on the particle surface depends on the surfactant type. The aggregate reorganization and growth in ferrofluids after 'PEGylation' [145] were observed (Figure 13). The SANS study was performed on mixed SO/polyethylene glycol (PEG) aqueous solutions in order to check the influence of a polymer additive on the surfactants behavior. SANS results revealed drastic morphological and interacting changes of micelles, due to the addition of PEG.

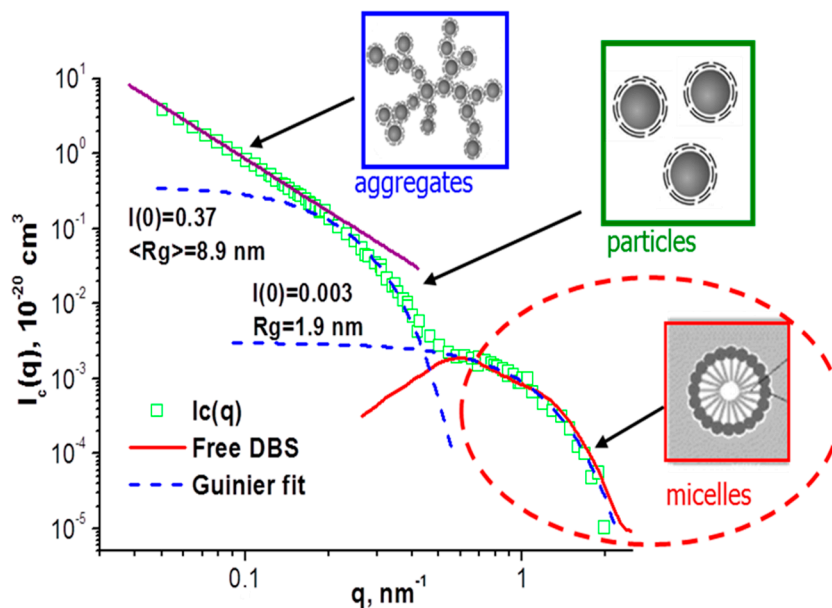


Figure 12. Complex structure of water-based ferrofluids with surfactant excess in its. Reprinted with permission from Reference [152].

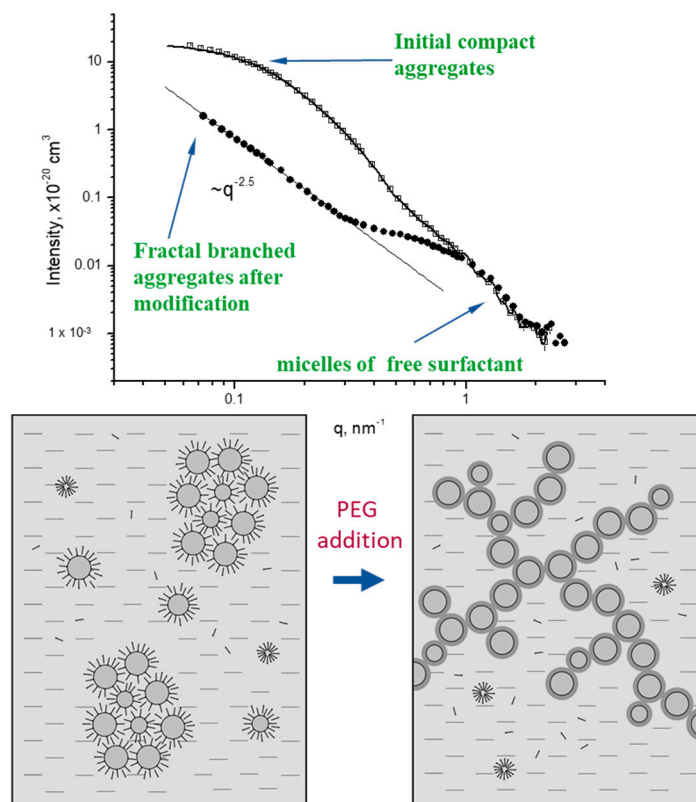


Figure 13. Ferrofluids with surfactant-polymer substitution: Change in aggregate structure according to small-angle neutron (SANS) analysis. SANS signals from different components in the solution were marked by arrows. Reprinted with permission from Reference [145] (<https://journals.iucr.org/>).

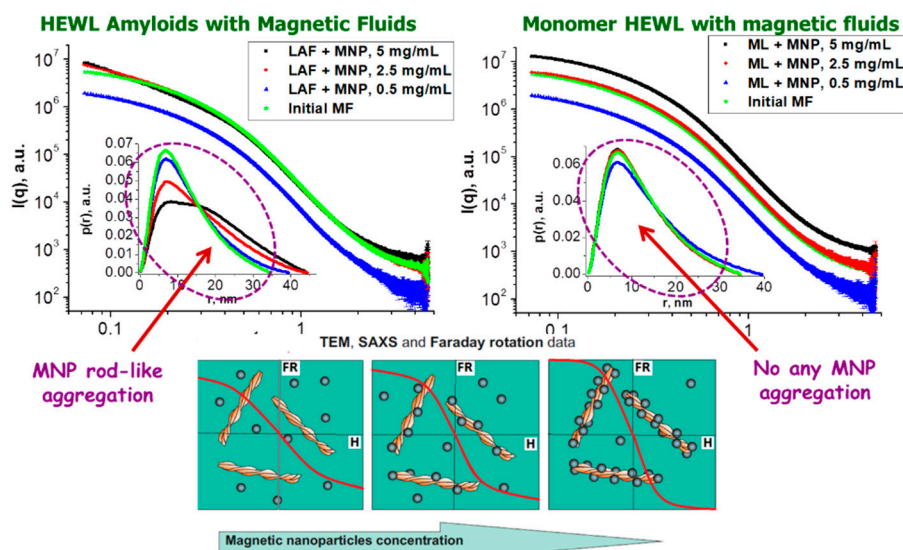


Figure 14. Behavior of magnetic nanoparticles in complex solutions of MNPs with amyloids (left) and with native (not aggregated) protein (right) according to small-angle X-ray scattering (SAXS) data. It's also shown formation of some rod-like aggregates in solutions of MNPs with amyloids and there is no any change in MNPs solutions with native protein at various MNPs concentrations. Sketch of the found adsorption of MNPs on amyloids surface with increase of MNPs concentration according to TEM, SAXS and optical (Faraday rotation) results (bottom). Reprinted with permission from Reference [151].

Neutron reflectometry used to obtain the SLD depth profiles investigated the assembly of magnetite nanoparticles in aqueous magnetic fluids close to a solid (silicon) surface under different external conditions (shear, magnetic field, etc.) [153–156]. The adsorption of surfactant coated magnetic nanoparticles from highly stable magnetic fluids on crystalline functionalized silicon was revealed from the specular reflectivity curves (Figure 15). The detailed analysis of the polarized neutron reflectometry data, together with SANS data, made it possible to obtain the magnetization depth profile and dependence of the resultant magnetic structure on the applied fields, including the distribution of NPs within the adsorption layer. Additionally, the impact of the solvent polarity, as well as bulk structure of ferrofluids, including particle concentration and particle geometry on the structural characteristics of the adsorption layer from magnetic fluids, was considered (Figure 15). The width of the adsorption layer is consistent with the size of single particles, thus showing the preferable adsorption of non-aggregated particles, in spite of the existing aggregate fraction in aqueous magnetic fluids. In the case of PEG-modified ferrofluids, the reorganization of MNP aggregates was observed, which correlates with the changes in the neutron reflectivity. It follows that the single adsorption layer of individual nanoparticles on the oxidized silicon surface for the initial magnetic fluids disappears after PEG modification. Consequently, in case of PEG modified magnetic fluid, all of the particles are in aggregates that are not adsorbed by silicon (Figure 15).

A comprehensive comparative study by small-angle neutron and X-ray scattering (SAXS and SANS) of water-based magnetic fluids with two different stabilization mechanisms—electrostatic (with citric acid (CA) Figure 16) and electro-steric (with oleic acid (OA) double layer; Figure 17)—over a large concentration range up to 30% hydrodynamic volume fraction, identified important differences on the microscopic level for these colloidal systems, as evidenced by the scattering curves in Figures 16 and 17. The electrostatic stabilization ensured high colloidal stability up to the highest magnetization 78.20 kA/m, while the electro-steric stabilized samples already show relatively large agglomerates at reduced volume fraction values [85].

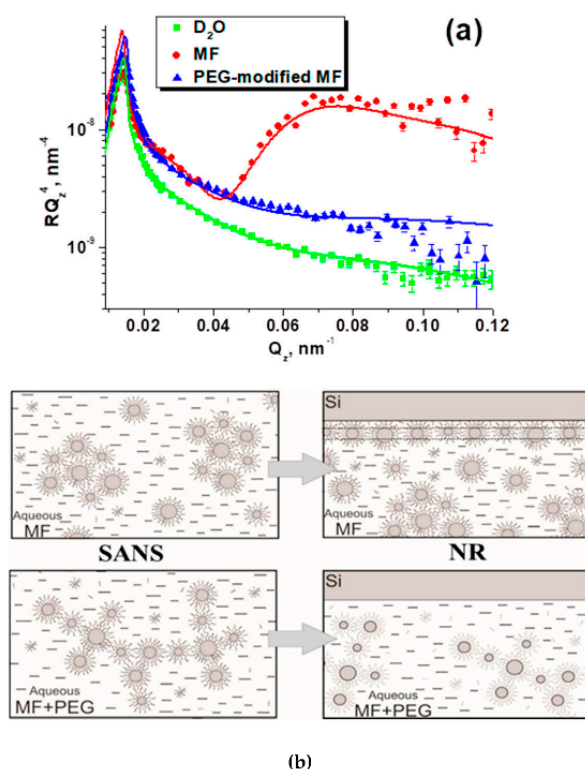


Figure 15. (a) Neutron reflectometry data for initial aqueous ferrofluids, PEG-modified ferrofluids and just buffer (D_2O) at interface with solid (Si). It could be seen that reflectivity curves for PEG-modified ferrofluids and just carrier (D_2O) are very similar and indicates on the absence of any nanoscale layer at interface. (b) Correlation between bulk structure of ferrofluids according to SANS and at interface ferrofluids/solid according to neutron reflectometry investigations. It is shown that there is no any adsorption of MNPs on solid in case of fractal branched aggregates in ferrofluids bulk. Reprinted with permission from Reference [153].

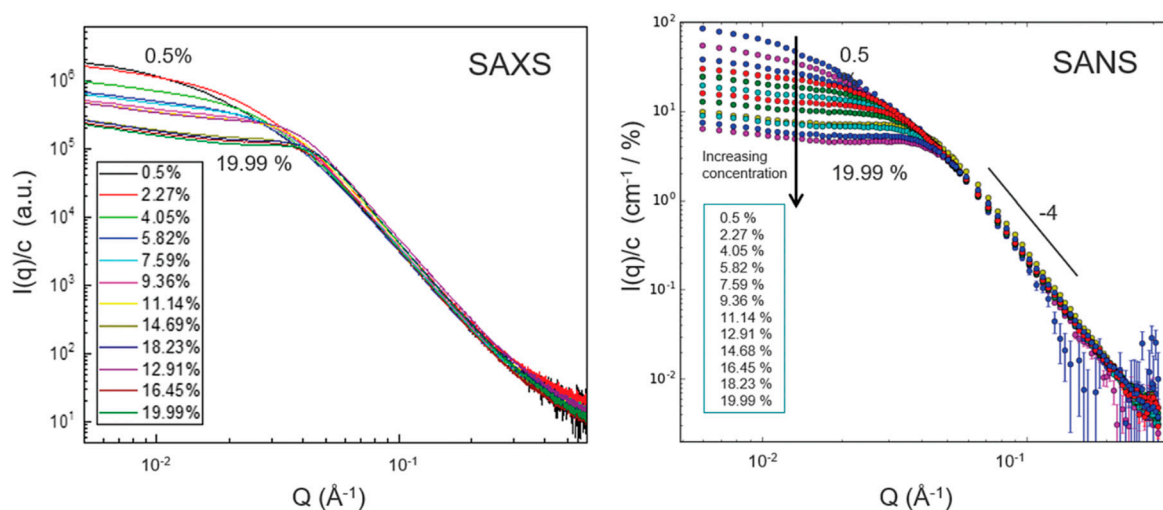


Figure 16. SAXS and SANS intensities normalized to the concentration of MNPs($\text{Fe}_3\text{O}_4/\text{CA}$) with varying concentration. The SANS data have been background-subtracted for the H_2O contribution. Reproduced from Reference [85] with permission from The Royal Society of Chemistry.

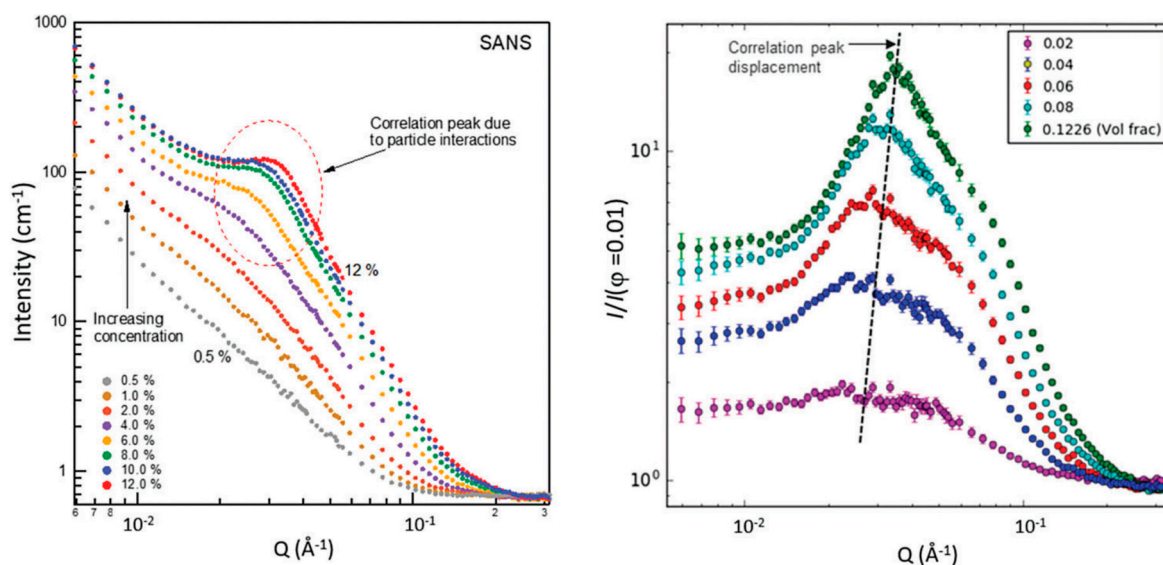


Figure 17. SANS data for the $\text{Fe}_3\text{O}_4/\text{OA}$ aqueous MF at different concentrations (left). Plot of the “apparent” structure factor (right). The SANS data have been divided by the data for a low-concentration sample (1%), without any further scaling. Reproduced from Reference [85] with permission from The Royal Society of Chemistry.

4.4.2. Light Scattering

Light scattering based structural characterization of magnetic colloids are an affordable laboratory table top alternative to SANS and SAXS. Therefore, a wide spectrum of equipment is already available on the market to help researchers with the fast and accurate characterization of magnetic colloids at nano and mesoscale, both spontaneous and magnetically induced.

Dynamic Light Scattering (DLS) uses the photon correlation spectroscopy to determine the colloidal particle hydrodynamic diameter from the time fluctuations of the light scattered by the colloid sample [157]. Static Light Scattering (SLS) uses the angle dependence of the scattered light intensity to determine the colloidal particle diameter via the Lorentz–Mie light scattering theory [158]. The spontaneous aggregation state of the nanoparticles in the colloid can be assessed while using DLS and SLS together with TEM and/or magnetogranulometry data.

Light scattering is also useful for the characterization of magnetically induced aggregation in magnetic colloids (Figure 18a). An ensemble of parallel prolate objects will scatter light in the plane perpendicular to their shape anisotropy axis, i.e., the scattering plane [158]. The polar angular dependence of the scattered light, i.e., the scattering pattern, can be measured on a projection plane perpendicular to the light propagation direction. 5 s interval scattering patterns from the application of 20 kA/m and 40 kA/m magnetic field, respectively, to a aqueous magnetic nanogel colloid are presented in Figure 17a top and Figure 18a bottom [35]. The scattering patterns themselves and their time evolution show the formation and growth of magnetically induced spindle-like (Figure 18b) aggregates in the colloid. The stronger the magnetic field, the more intense the scattering pattern, and, thus, the more voluminous the aggregated phase. Magnetically induced aggregation in magnetic colloids is of primary concern for practical application due to the potential catastrophic loss of specific surface and/or blood vessels clogging during in vivo experiments. Mesoscale aggregation in magnetic colloids leads to the formation of magnetic field oriented spindle like clusters (Figure 18b), with thickness in the order of microns and lengths in the order of tens to hundreds microns [35,63]. Recently, it was discovered that large scale structuring could be induced by high frequency magnetic fields with amplitude as low as 40 Oe, in suspensions of magnetic multicore-shell nanoparticles (MMCS) [159].

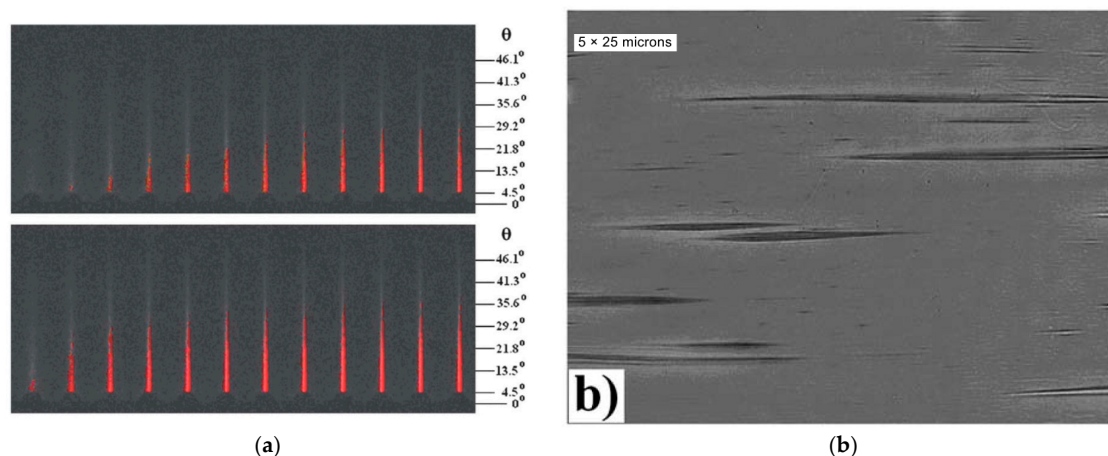


Figure 18. (a) Light scattering patterns at 5 s intervals after field onset for 20 kA/m (top) and 40 kA/m (bottom) and (b) Optical microscopy image of magnetically induced spindle like aggregates (the scale bar is 25 microns). Reprinted with permission from Reference [35].

Although this large scale structuring can be observed with optical microscopy, light scattering offers the advantage of determining the magnetic supersaturation of the colloid, i.e., the magnetic field dependence of the weight of nanoparticles contained in the aggregates [35].

Figure 19 presents the magnetic field dependence of the supersaturation in three types of MMCS dispersions. The 40 kA/m DC field supersaturation for aqueous dispersions of 60 nm MMCS hardly reaches 0.1% (Figure 19a), while, for 100 nm, MMCSs reach almost 50% (Figure 19b). A 10 kA/m amplitude 100 kHz AC field induces almost 80% supersaturation in 250 nm MMCS dispersion (Figure 19c). Thus, the shear magnitude of the aggregation phenomena should be a priority concern for any practical applications, depending on the composite size and magnetic field intensity.

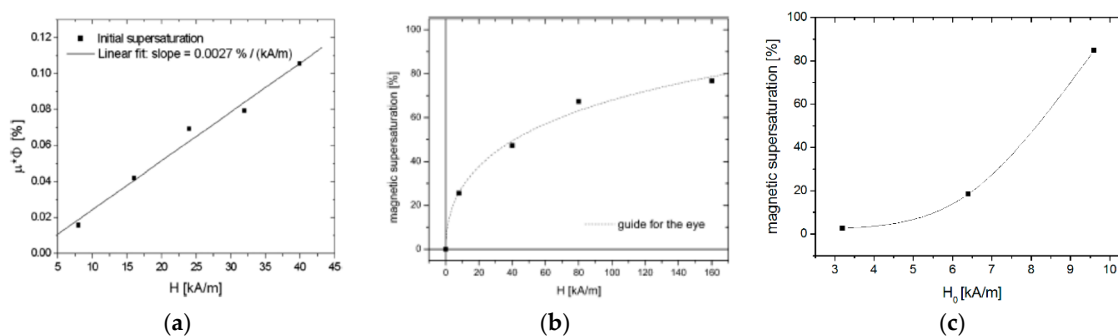


Figure 19. Magnetic field dependence of supersaturation for: (a) 60 nm magnetic multicore-shell nanoparticles (MMCS) in DC field. Reprinted with permission from Reference [35], (b) 100 nm MMCS in DC field. Reprinted with permission from Reference [63], and (c) 250 nm MMCS in AC field [159].

4.5. Rheology and Magnetorheology of Aqueous Ferrofluids

In the case of aqueous bio-ferrofluids usually the multi-core particles in the 50–100 nm size range are predominant. Additionally, while bio-ferrofluids are highly diluted, vector magnetometry and SANS data indicate field dependent “colloidal” anisotropies that arise from the competition between steric repulsion and magnetostatic attraction between particles, having a significant influence on the magnetorheology of these colloids [160].

In the case of concentrated ferrofluids, achieving a high saturation magnetization value requires the increase of physical volume fraction and, thus, a corresponding increase of the hydrodynamic volume fraction, however to different extents, depending on the stabilization mechanism, electrostatic or electro-steric [161]. The electrostatically stabilized ferrofluids have the advantage of reducing the

total suspended material at constant magnetic volume fraction when compared with a surfactant stabilized fluid [162], due to the much greater thickness of the steric stabilizing layer.

Vasilescu and colab. made an in-depth analysis on two basic types of water based magnetic fluids (MFs), containing magnetite nanoparticles with electrostatic and with electro-steric stabilization, both being obtained by chemical coprecipitation synthesis under atmospheric conditions [85]. The two sets of magnetic fluid samples, one with citric acid (MF/CA) and the other with oleic acid (MF/OA) coated magnetic nanoparticles, respectively, achieved saturation magnetization values $M_S = 78.20$ kA/m for the electrostatically and $M_S = 48.73$ kA/m for the electro-sterically stabilized aqueous ferrofluids, which are among the highest reported to date. These fluids show both similarities and important differences in their microscopic and macroscopic properties.

The two types of ferrofluids manifest different structuring behavior, as evidenced by small angle scattering investigations (Figures 16 and 17); therefore, significant differences are expected in their magnetorheology, in particular concerning the magnitude of the magnetoviscous effect (expressed as the relative field-induced change of viscosity in the presence of a magnetic field, $(\eta_H - \eta_{H=0})/\eta_{H=0}$).

The most concentrated electro-steric stabilized (oleic acid) magnetic fluid sample (MF/OA9) shows shear-thinning (pseudoplastic), both in zero and non-zero magnetic fields—Figure 20, due to particle agglomerates that are progressively destroyed at increasing shear rate values. The applied field induces the formation of new agglomerates, besides those already existing in zero field, as evidenced by the observed magnetoviscous effect (MVE). After demagnetization, the viscosity values remain slightly increased with respect to the initial values, which shows that the agglomerates that formed in the applied field do not fall apart when the field is switched off (are irreversible at the characteristic timescale of measurements).

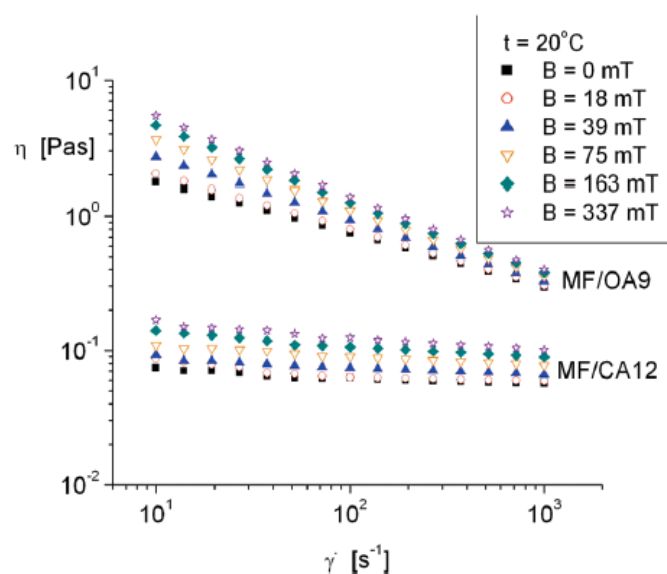


Figure 20. Viscosity curves at different magnetic flux densities for the highest concentration samples: MF/CA12 (physical vol fraction 20%) and MF/OA9 (physical vol fraction 14%). Reproduced from Reference [85] with permission from The Royal Society of Chemistry.

The electrostatic stabilized (citric acid) highest concentration magnetic fluid sample (MF/CA12) has an approximately Newtonian behavior in zero and non-zero magnetic field—Figure 20. From viscosity curves, the MVE is relatively reduced and almost independent of the shear rate. Furthermore, the magnetic field induced agglomeration of particles is partly irreversible; after demagnetization, the viscosities are somewhat higher than the initial values. Moreover, at $B = 337$ mT, the sample becomes slightly pseudoplastic.

Representing MVE vs. shear rate and vs. magnetic field induction (Figure 21a,b), it was observed that, for small shear rates, the magnetoviscous effect is considerably higher for the MF/OA9 sample.

At shear rates $\gamma > 10^2 \cdot \text{s}^{-1}$, the situation changes and the MVE is somewhat greater for the MF/CA12 sample, which indicates the existence of loosely bound agglomerates in the OA stabilized sample, which are disrupted by increasing the shear rate. Abrupt and irreversible changes of the effective viscosity in magnetic fields, which would reflect magnetic field induced phase separation, were not observed. The MVE of the citric acid stabilized magnetic fluid sample is mainly determined by the physical particle volume fraction, which is approx. two times higher than that of the oleic acid stabilized sample.

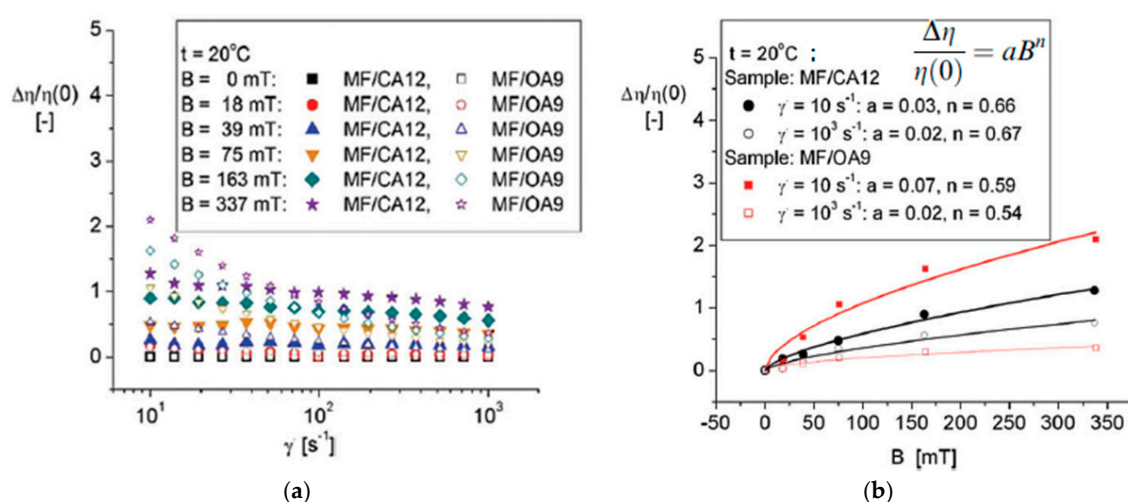


Figure 21. (a) Magnetoviscous effect (MVE) dependence on the shear rate at different magnetic flux densities; (b) MVE dependence on the magnetic flux density at two shear rate values. Reproduced from Reference [85] with permission from The Royal Society of Chemistry.

In good correlation with the results of small-angle scattering, the MVE values at low shear rates were found to be more pronounced for the MF/OA9 sample than for the MF/CA12 sample, which denotes the presence of agglomerates (the existence of correlations) already at small volume fraction values in the case of MF/OA magnetic fluids. However, the observed viscosity increase is moderate when compared to the more than an order of magnitude increase of the effective viscosity in the case of bio-ferrofluids [16].

Bio-ferrofluids having multi-core particles [40,52,53,163–166] demonstrated an increasing interest for the biomedical area during the last years. The higher particle diameter, still guaranteeing a stable suspension, but without magnetized clumps of particles that are caused by remanence, allows for a more effective collection of the particles by the liver. Ferrofluids with multicore particles manifest a rather strong magnetorheological effect, despite the comparatively low concentration of magnetic nanoparticles specific to nanomedicine applications [167,168]. As the concentration of MNPs in blood flow is rather low, for the simulation of the rheological behavior the investigation of dilute ferrofluids is a first step [164,168], including MVE measurements. Nowak and Odenbach developed a capillary viscometer [167], providing a flow situation comparable to the flow in a blood vessel, and having the range of the shear rates adapted to what is expected in the human organism due to the very low zero field viscosity and for a realistic evaluation of MVE. The special capillary viscometer proved to be suitable for measuring the magnetoviscous effect in bio-ferrofluids and the results show good correlation with data measured by rotational rheometry—Figure 22.

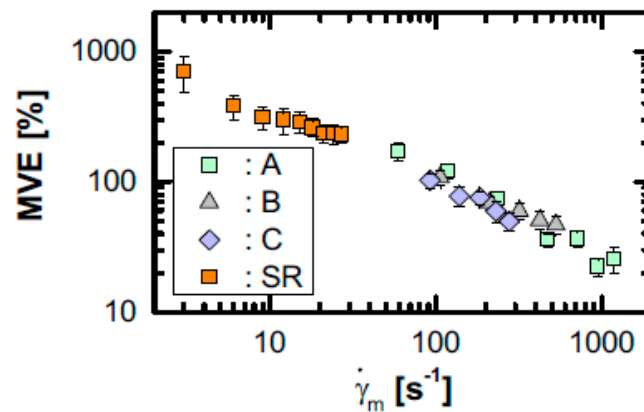


Figure 22. Comparison of MVE data obtained with the capillary viscometer (for three capillaries A, B, C) and with cone-plate setup by rotational rheometry (SR) at the magnetic field strength $H = 30$ kA/m. Reprinted with permission from Reference [167].

The data from Figure 22 refer to a stable bio-ferrofluid fluidMAG-D-100 nm manufactured by Chemicell GmbH (Berlin, Germany) composed of magnetite as a core material, with starch as surfactant (hydrodynamic diameter was 100 nm, mean single particle diameter was 15.9 nm), and have a concentration in suspension of 25 mg mL^{-1} , a sample also previously investigated in [16].

There are several parameters of the suspended nanoparticles that influence the MVE: the core diameter of the particles, the thickness of the surfactant layer, and the spontaneous magnetization M_0 . Regarding the influence of these parameters, in [167] the MVE was compared for three biocompatible ferrofluids with identical composition, except in relation to their hydrodynamic diameter and core composition: the fluidMAG-D-50 nm contains single core particles (hydrodynamic diameter 50 nm), while the other two feature multicore particles: fluidMAG-D-100 nm and fluidMAG-D-200 nm (hydrodynamic diameter 100 nm and 200 nm).

No manifestation of any MV effect was observed for the fluid with single core particles, fluidMAG-D-50 nm. Indeed, the interaction parameter for this ferrofluid

$$\lambda^* = \frac{\mu_0 M_0^2 d^3 \pi}{144 k_B T} \left(\frac{d}{d+2s} \right)^3 \quad (1)$$

was very small: $\lambda^* = 0.09$, and a particle interaction (and implicitly for MVE) is only expected for values of the interaction parameter $\lambda^* > 1$. Here, M_0 is the spontaneous magnetization, μ_0 —the vacuum permeability, k_B —the Boltzmann constant, T —the temperature, d —the core diameter, and s —the surfactant thickness.

For the other two ferrofluids that consist of multicore particles, the interaction parameter was calculated with [169]:

$$\lambda_{MC} = \frac{\mu_0 \mu_F \beta^2 (d/2)^3 H_0^2 \pi}{2 k_B T} \left(\frac{d}{d+2s} \right)^3, \quad \text{where } \beta = \frac{\mu_P - \mu_F}{\mu_P + 2\mu_F} \quad (2)$$

in which μ_F represents the relative permeability of the fluid, μ_P —the particles' relative permeability, β —the magnetic contrast factor, and H_0 —the magnetic field strength. The interaction parameter at $H = 10$ kA/m has the values: $\lambda_{MC} = 1.08$ for fluidMAG-D-100 nm and $\lambda_{MC} = 20.1$ for fluidMAG-D-200 nm, which ensures a great MVE—Figure 23.

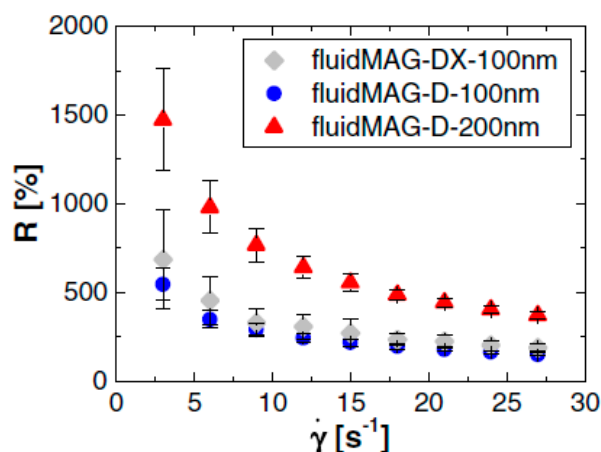


Figure 23. The shear rate dependence of the MVE of three ferrofluid samples at $H = 30$ kA/m. The commercial fluidMAG-DX-100 nm, investigated in previous studies [167,168], has multicore particles with hydrodynamic diameter 100 nm and stabilized with dextran. Reprinted with permission from Reference [164].

It can be observed from Figure 23 that MVE strongly increases with increasing hydrodynamic diameter, which proves the strong influence of the microscopic makeup of the fluid on this effect. The difference of approx. 20% for MVE for samples fluidMAG-DX-100 nm and fluidMAG-D-100 nm is most likely due to different surfactants (dextran, respective starch) and to different thicknesses of surfactant layers. In addition, MVE increases with intensifying of the magnetic field, due to increasing magnetic interactions between the particles, according to the previously mentioned interaction parameter λ_{MC} , favoring particle agglomeration—Figure 24—and the MVE decreases with increasing shear rate—Figures 23 and 24—due to the rupturing of chain-like structures induced by the magnetic field.

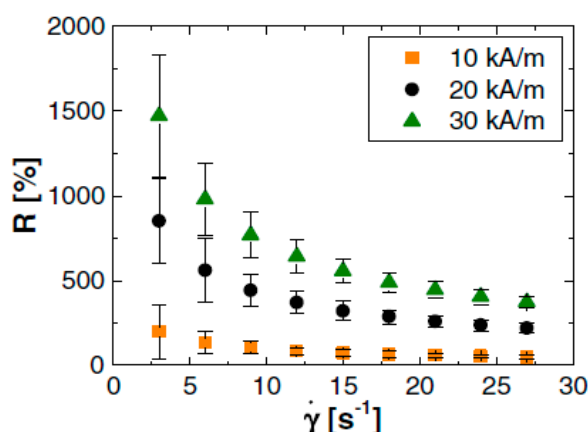


Figure 24. The MVE of the ferrofluid fluidMAG-D-200 nm for three magnetic field strengths depending on the shear rate. Reprinted with permission from Reference [164].

Nowak et al. [167] have comparatively investigated a dilution series starting from two bio-ferrofluids to determine direct connections between the microscopic make-up and the actual rheological behavior as well to establish a condition comparable with the concentration of the fluids in blood flow during the biomedical application: fluidMAG-DX-100 nm (GmbH, Berlin, Germany) and FF054L (provided by the research group of Prof. Alexiou, Erlangen, Germany). Both ferrofluids are based on multi-core magnetite/maghemite particles with 100 nm mean particle diameter. Both ferrofluids have Newtonian behavior in the absence of a magnetic field—Figure 25.

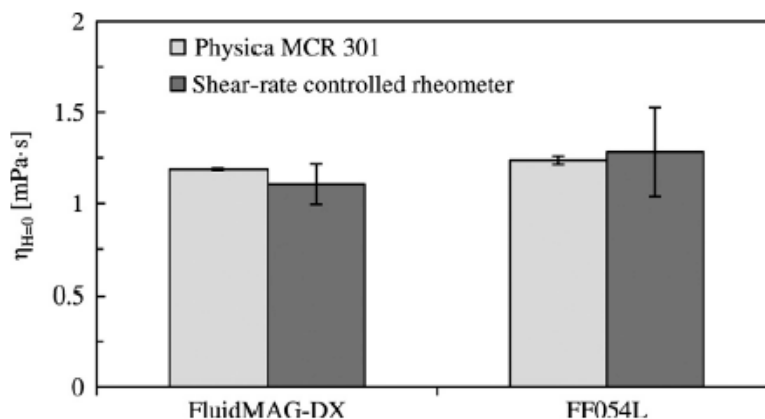


Figure 25. Newtonian viscosity of fluidMAG-DX-100 nm and FF054L samples without the influence of a magnetic field. Reprinted with permission from Reference [16].

The measurements revealed that the magnetorheology of these samples is quite similar; their behavior becomes shear-thinning and MVE is great and strongly dependent on magnetic field intensity—Figure 26.

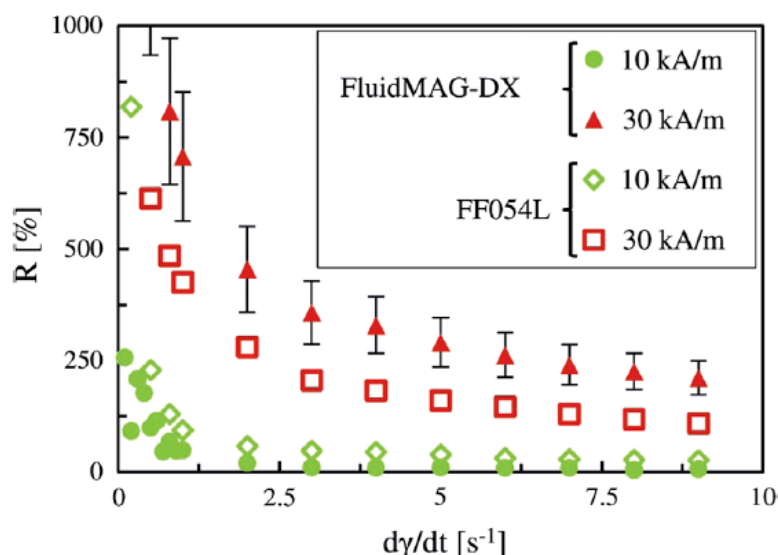


Figure 26. The MVE in the fluidMAG-DX-100 nm in comparison with the FF054L for two values of intensity of magnetic field. Reprinted with permission from Reference [16].

At $H = 10$ kA/m It is observed from Figure 26 that the MVE is higher for FF054L, despite its lower concentration of suspended magnetic material (0.12% vs. 0.28% in fluidMAG-DX-100 nm). For $H > 10$ kA/m, the effect is higher for the commercial fluid MAG-DX, as shown in Figure 26 for $H = 30$ kA/m. This change in the strength of the MVE for the two fluids can be understood while referring to the particle size distribution (a slightly higher fraction of larger particles in the FF054L fluid) as well as to the parameters of the investigated ferrofluids (saturation magnetization: $M_S = 1275.5$ A/m for fluidMAG-DX-100 nm and $M_S = 520.77$ A/m for FF054L, volume fraction of magnetic material: $\Phi = 0.28\%$ for fluidMAG-DX-100 nm and $\Phi = 0.12\%$ for FF054L), and to the size dependence of the interparticle interaction. The stronger MVE of the FF054L at low field strength is related to the slightly wider particle size distribution involving comparatively larger particles that can contribute to the formation of chains at a $H = 10$ kA/m. On the contrary, at $H > 10$ kA/m, the higher volume fraction of magnetic material in fluidMAG-DX-100 nm leads to a stronger MVE in this fluid.

For most biomedical applications, the ferrofluids are supposed to a dilution after injection into the blood flow; therefore, both samples investigated in [16] were diluted with distilled water. Measurements for the dilution series revealed that there is still a strong MVE for a dilution factor $K < 5$ ($K = (V_{FF} + V_{diluting\ agent})/V_{FF}$)—when magnetoviscous effect exceeds about 300%, but, if $K > 10$, the MVE is hardly detectable. For diluted ferrofluids, the shear dependency of the MVE is still manifestly present.

5. Concluding Remarks and Theranostic Prospects

The development of various nanoparticle systems for nanomedicine is a challenging task of present day's material science. In this context, iron oxide nanoparticle systems are among of the most promising nanomaterials in clinical diagnostic and therapeutic applications (theranostics); therefore, the review was focused on efficient manufacturing procedures and manifold characterization methods of these magneto-responsive systems. The recent progress in designed synthesis and multiple functional coating of single- and multicore magnetic nanocomposite particles for imaging, drug delivery, hyperthermia, or point-of-care diagnostics was thoroughly evaluated in correlation with the results of advanced physical-chemical characterization methods, among them X-ray photoelectron spectroscopy, AC susceptometry, small-angle neutron and X-ray scattering, neutron reflectometry, and magnetorheology, beside the more frequently used techniques, such as high resolution transmission electron microscopy, dynamic and static light scattering, or zeta potential measurements. The reviewed manifold physical, chemical, and colloidal characterization is undoubtedly required in order to ensure the desired outcome in the near future of standardized manufacturing of magnetic nanoparticle systems for nanomedicine applications before the translation of novel laboratory creation into the viable clinical product including safety, regulatory, and ethical requirements.

Author Contributions: Writing—original draft, Writing—review & editing, V.S.; Conceptualization, Writing—original draft, D.P., M.V.A. and R.T.; Writing—original draft, V.I.P., D.S.-R. and T.S.; Conceptualization, Writing—original draft, Writing—review & editing, E.T.; Conceptualization, Writing—original draft, Writing—review & editing, Supervision, L.V. All authors have read and agree to the published version of the manuscript.

Funding: The work of D.S.-R., L.V. and V.S. was mainly supported by the RA-TB/CFATR/LMF multiannual research program 2016–2020 and by a grant of the Romanian Ministry of Research and Innovation, CCCDI-UEFISCDI, project number PN-III-PI-1,2-PCCDI-2017-0871, contract c47PCCDI/2018. D.P., L.V. and V.S. are indebted for the partial support from the bilateral agreement between Romanian Academy and Italian National research Council project *Ferro-Tera*. R.T. acknowledges the support from the grant of the Romanian Ministry of Research and Innovation, CCCDI-UEFISCDI, project number PN-III-P1-1.2-PCCDI-2017-0769, contract no. 64, within PNCDI III and from the JINR-RO project 04-4-1121-2015/2020. The work of E.T. and T.S. was supported by the Hungarian National Research, Development and Innovation Office via the Grants FK-124851.

Conflicts of Interest: The authors declare no conflict of interest.

References

1. Pelaz, B.; Alexiou, C.; Alvarez-Puebla, R.A.; Alves, F.; Andrews, A.M.; Ashraf, S.; Bosi, S.; Carril, M.; Chen, C.; Cheng, Z.; et al. Diverse Applications of Nanomedicine. *ACS Nano* **2017**, *11*, 2313–2381. [[CrossRef](#)] [[PubMed](#)]
2. Thanh, N.T.K. (Ed.) *Clinical Applications of Magnetic Nanoparticles Design to Diagnosis Manufacturing to Medicine*; CRC Press Taylor & Francis Group: Boca Raton, FL, USA, 2018.
3. Colombo, M.; Carregal-Romero, S.; Casula, M.F.; Gutiérrez, L.; Morales, M.P.; Böhm, I.B.; Heverhagen, J.T.; Prosperi, D.; Parak, W.J. Biological applications of magnetic nanoparticles. *Chem. Soc. Rev.* **2012**, *41*, 4306–4334. [[CrossRef](#)] [[PubMed](#)]
4. Kuncser, V.; Palade, P.; Kuncser, A.; Greculeasa, S.; Schinteie, G. Engineering Magnetic Properties of Nanostructures via Size Effects and Interphase Interactions. In *Size Effects in Nanostructures*; Kuncser, V., Miu, L., Eds.; Springer: Berlin, Germany, 2014; pp. 169–237.
5. Wells, J.; Kazakova, O.; Posth, O.; Steinhoff, U.; Petronis, S.; Bogart, L.K.; Southern, P.; Pankhurst, Q.; Johansson, C. Standardisation of magnetic nanoparticles in liquid suspension. *J. Phys. D Appl. Phys.* **2017**, *50*, 383003–28. [[CrossRef](#)]

6. Bogren, S.; Fornara, A.; Ludwig, F.; Morales, M.P.; Steinhoff, U.; Hansen, M.F.; Kazakova, O.; Johansson, C. Classification of Magnetic nanoparticle systems—synthesis, standardization and analysis methods in the NanoMag project. *Int. J. Mol. Sci.* **2015**, *16*, 20308–20325. [[CrossRef](#)]
7. Nedyalkova, M.; Donkova, B.; Romanova, J.; Tzvetkov, G.; Madurga, S.; Simeonov, V. Iron oxide nanoparticles—In vivo/in vitro biomedical applications and in silico studies. *Adv. Colloid Interface Sci.* **2017**, *249*, 192–212. [[CrossRef](#)]
8. Song, C.; Sun, W.; Xiao, Y.; Shi, X. Ultrasmall iron oxide nanoparticles: Synthesis, surface modification, assembly, and biomedical applications. *Drug Discov. Today* **2019**, *24*, 835–844. [[CrossRef](#)]
9. Roca, A.G.; Gutiérrez, L.; Gavilán, H.; Brollo, M.E.F.; Veintemillas-Verdaguer, S.; Morales, M.P. Design strategies for shape-controlled magnetic iron oxide nanoparticles. *Adv. Drug Deliv. Rev.* **2019**, *138*, 68–104. [[CrossRef](#)]
10. Savliwala, S.; Chiu-Lam, A.; Unni, M.; Rivera-Rodriguez, A.; Fuller, E.; Sen, K.; Threadcraft, M.; Rinaldi, C. Magnetic nanoparticles. In *Nanoparticles for Biomedical Applications: Fundamental Concepts, Biological Interactions and Clinical Applications*; A Volume in Micro and Nano Technologies; Chapter 13; Chung, E.J., Leon, L., Rinaldi, C., Eds.; Elsevier: Amsterdam, The Netherlands, 2019; pp. 195–221.
11. Sun, Z.; Worden, M.; Thliveris, J.A.; Hombach-Klonisch, S.; Klonisch, T.; van Lierop, J.; Hegmann, T.; Miller, D.W. Biodistribution of negatively charged iron oxide nanoparticles (IONPs) in mice and enhanced brain delivery using lysophosphatidic acid (LPA). *Nanomed. Nanotechnol. Biol. Med.* **2016**, *12*, 1775–1784. [[CrossRef](#)]
12. Khandhar, A.P.; Keselman, P.; Kemp, S.J.; Ferguson, R.M.; Goodwill, P.W.; Conolly, S.M.; Krishnan, K.M. Evaluation of PEG-coated iron oxide nanoparticles as blood pool tracers for preclinical Magnetic Particle Imaging. *Nanoscale* **2017**, *9*, 1299–1306. [[CrossRef](#)]
13. Gul, S.; Khan, S.B.; Rehman, I.U.; Khan, M.A.; Khan, M.I. A Comprehensive Review of Magnetic Nanomaterials Modern Day Theranostics. *Front. Mater.* **2019**, *6*, 179. [[CrossRef](#)]
14. Kostopoulou, A.; Lappas, A. Colloidal magnetic nanocrystal clusters: Variable length-scale interaction mechanisms, synergetic functionalities and technological advantages. *Nanotechnol. Rev.* **2015**, *4*, 595–624. [[CrossRef](#)]
15. Muscas, G.; Yaacoub, N.; Concas, G.; Sayed, F.; Sayed Hassan, R.; Greneche, J.M.; Cannas, C.; Musinu, A.; Foglietti, V.; Casciardi, S.; et al. Evolution of the magnetic structure with chemical composition in spinel iron oxide nanoparticles. *Nanoscale* **2015**, *7*, 13576–13585. [[CrossRef](#)] [[PubMed](#)]
16. Nowak, J.; Wolf, D.; Odenbach, S. A rheological and microscopical characterization of biocompatible ferrofluids. *J. Magn. Magn. Mater.* **2014**, *354*, 98–104. [[CrossRef](#)]
17. Vékás, L.; Avdeev, M.V.; Bica, D. Magnetic nanofluids: Synthesis and structure. In *Nanoscience in Biomedicine*; Shi, D., Ed.; Springer: Berlin, Germany, 2009; pp. 650–720.
18. Susan-Resiga, D.; Socoliuc, V.; Boros, T.; Borbáth, T.; Marinica, O.; Han, A.; Vékás, L. The influence of particle clustering on the rheological properties of highly concentrated magnetic nanofluids. *J. Colloid Interface Sci.* **2012**, *373*, 110–115. [[CrossRef](#)]
19. Silva, A.K.A.; Di Corato, R.; Gazeau, F.; Pellegrino, T.; Wilhelm, C. Magnetophoresis at the nanoscale: Tracking the magnetic targeting efficiency of nanovectors. *Nanomedicine* **2012**, *7*, 1–15.
20. Shliomis, M.I. Magnetic fluids. *Sov. Phys. Usp.* **1974**, *17*, 153. [[CrossRef](#)]
21. Krishnan, K.M. Biomedical Nanomagnetism: A Spin through Possibilities in Imaging, Diagnostics, and Therapy. *IEEE Trans. Magn.* **2010**, *46*, 2523–2558. [[CrossRef](#)]
22. Dutz, S.; Hergt, R. Magnetic particle hyperthermia—A promising tumour therapy? *Nanotechnology* **2014**, *25*, 452001–452028. [[CrossRef](#)]
23. Wiekhorst, F.; Steinhoff, U.; Eberbeck, D.; Trahms, L. Magnetorelaxometry assisting biomedical applications of magnetic nanoparticles. *Pharm. Res.* **2012**, *29*, 1189–1202. [[CrossRef](#)]
24. Ivanov, A.O.; Kantorovich, S.S.; Reznikov, E.N.; Holm, C.; Pshenichnikov, A.F.; Lebedev, A.V.; Chremos, A.; Camp, P.J. Magnetic properties of polydisperse ferrofluids: A critical comparison between experiment, theory, and computer simulation. *Phys. Rev. E* **2007**, *75*, 061405. [[CrossRef](#)]
25. Suber, L.; Peddis, D. Approaches to synthesis and characterization of spherical and anisometric metal oxide magnetic nanomaterials. In *Magnetic Nanomaterials*; Kumar, C., Ed.; WILEY-VCH Verlag GmbH & Co. KGaA: Weinheim, Germany, 2010; Volume 4, Chapter 12; pp. 431–487.

26. Peddis, D. Magnetic Properties of Spinel Ferrite Nanoparticles: Influence of the Magnetic Structure. In *Magnetic Nanoparticle Assemblies*; Trohidou, K.N., Ed.; Pan Stanford Publishing: Singapore, 2014; Volume 7, pp. 978–981.
27. Dormann, J.L.; Fiorani, D. (Eds.) *Magnetic Properties of Fine Particles*, 1st ed.; North-Holland Delta Series; Elsevier Science Publishers B.V.: Amsterdam, The Netherlands, 1992.
28. Crangle, J. *Solid State Magnetism*; Great Britain Edward Arnold: London, UK, 1991.
29. Coey, J.M.D. *Magnetism and Magnetic Materials*; Cambridge University Press: New York, NY, USA, 2010.
30. Bodker, F.; Morup, S.; Linderroth, S. Surface Effects in Metallic Iron Nanoparticles. *Phys. Rev. Lett.* **1994**, *72*, 282. [[CrossRef](#)] [[PubMed](#)]
31. Muscas, G.; Yaacoub, N.; Peddis, D. Chapter 4—Magnetic Disorder in Nanostructured Materials. In *Novel Magnetic Nanostructures Rentschler*; Domracheva, N., Caporali, M., Eva, B.T., Eds.; Elsevier: Amsterdam, The Netherlands, 2018; pp. 127–163.
32. Daou, T.J.; Greneche, J.M.; Pourroy, G.; Buathong, S.; Derory, A.; Ulhaq-Bouillet, C.; Donnio, B.; Guillon, D.; Begin-Colin, S. Coupling Agent Effect on Magnetic Properties of Functionalized Magnetite-Based Nanoparticles. *Chem. Mater.* **2008**, *20*, 5869–5875. [[CrossRef](#)]
33. Peddis, D.; Orrù, F.; Ardu, A.; Cannas, C.; Musinu, A.; Piccaluga, G. Interparticle Interactions and Magnetic Anisotropy in Cobalt Ferrite Nanoparticles: Influence of Molecular Coating. *Chem. Mater.* **2012**, *24*, 1062–1071. [[CrossRef](#)]
34. Vasilakaki, M.; Ntallis, N.; Yaacoub, N.; Muscas, G.; Peddis, D.; Trohidou, K.N. Optimising the Magnetic Performance of Co Ferrite Nanoparticles via Organic Ligand Capping. *Nanoscale* **2018**, *10*, 21244–21253. [[CrossRef](#)] [[PubMed](#)]
35. Socoliuc, V.; Vékás, L.; Turcu, R. Magnetically induced phase condensation in an aqueous dispersion of magnetic nanogels. *Soft Matter* **2013**, *9*, 3098–3105. [[CrossRef](#)]
36. Bernad, S.I.; Susan-Resiga, D.; Vekas, L.; Bernad, E.S. Drug targeting investigation in the critical region of the arterial bypass graft. *J. Magn. Magn. Mater.* **2019**, *475*, 14–23. [[CrossRef](#)]
37. Bernad, S.I.; Susan-Resiga, D.; Bernad, E.S. Hemodynamic Effects on Particle Targeting in the Arterial Bifurcation for Different Magnet Positions. *Molecules* **2019**, *24*, 2509. [[CrossRef](#)]
38. Ge, J.; Hu, Y.; Biasini, M.; Beyermann, W.P.; Yin, Y. Superparamagnetic magnetite colloidal nanocrystal clusters. *Angew. Chem. Int. Ed.* **2007**, *46*, 4342–4345. [[CrossRef](#)]
39. O'Mahony, J.J.; Platt, M.; Kilinc, D.; Lee, G. Synthesis of superparamagnetic particles with tunable morphologies: The role of nanoparticle-nanoparticle interactions. *Langmuir* **2013**, *29*, 2546–2553. [[CrossRef](#)]
40. Yoon, K.Y.; Mehrmohammadi, M.; Borwankar, A.; Emelianov, S.Y.; Johnston, K.P. Synthesis of Iron Oxide Nanoclusters with Enhanced Magnetization and Their Applications in Pulsed Magneto-Motive Ultrasound Imaging. *NANO Brief Rep. Rev.* **2015**, *10*, 1550073. [[CrossRef](#)]
41. Tombácz, E.; Turcu, R.; Socoliuc, V.; Vékás, L. Magnetic iron oxide nanoparticles: Recent trends in design and synthesis of magneto-responsive nanosystems. *Biochem. Biophys. Res. Comm.* **2015**, *468*, 442–453. [[CrossRef](#)] [[PubMed](#)]
42. Charles, S.W. The preparation of magnetic fluids. In *Ferrofluids*; Odenbach, S., Ed.; Springer: Berlin, Germany, 2002; pp. 3–18.
43. Veiseh, O.; Gunn, J.W.; Zhang, M. Design and fabrication of magnetic nanoparticles for targeted drug delivery and imaging. *Adv. Drug Deliv. Rev.* **2010**, *62*, 284–304. [[CrossRef](#)] [[PubMed](#)]
44. Gupta, A.K.; Gupta, M. Synthesis and surface engineering of iron oxide nanoparticles for biomedical applications. *Biomaterials* **2005**, *26*, 3995–4021. [[CrossRef](#)] [[PubMed](#)]
45. Laurent, S.; Forge, D.; Port, M.; Roch, A.; Robic, C.; Vander Elst, L.; Muller, R.N. Magnetic Iron Oxide Nanoparticles: Synthesis, Stabilization, Vectorization, Physicochemical Characterizations, and Biological Applications. *Chem. Rev.* **2008**, *108*, 2064–2110. [[CrossRef](#)]
46. Tartaj, P.; Morales, M.P.; Veintemillas-Verdaguer, S.; Gonzalez-Carreno, T.; Serna, C.J. Synthesis, Properties and Biomedical Applications of Magnetic Nanoparticles. *Handb. Magn. Mater.* **2006**, *16*, 403–482.
47. Oh, J.K.; Park, J.M. Iron oxide-based superparamagnetic polymeric nanomaterials: Design, preparation, and biomedical application. *Prog. Polym. Sci.* **2011**, *36*, 168–189. [[CrossRef](#)]
48. Baaziz, W.; Pichon, B.P.; Fleutot, S.; Liu, Y.; Lefevre, C.; Grenéche, J.-M.; Toumi, M.; Mhiri, T.; Begin-Colin, S. Magnetic iron oxide nanoparticles: Reproducible tuning of the size and nanosized-dependent composition, defects, and spin canting. *J. Phys. Chem. C* **2014**, *118*, 3795–3810. [[CrossRef](#)]

49. Bica, D.; Vékás, L.; Avdeev, M.; Marinică, O.; Socoliuc, V.; Bălăsoiu, M.; Garamus, V.M. Sterically stabilized water based magnetic fluids: Synthesis, structure and properties. *J. Magn. Magn. Mater.* **2007**, *311*, 17–21. [[CrossRef](#)]
50. Herranz, F.; Morales, M.P.; Roca, A.G.; Desco, M.; Ruiz-Cabello, J. A new method for the rapid synthesis of water stable superparamagnetic nanoparticles. *Chem. A Eur. J.* **2008**, *14*, 9126–9130. [[CrossRef](#)]
51. Palma, S.I.C.J.; Marciello, M.; Carvalho, A.; Veintemillas-Verdaguer, S.; Puerto Morales, M.; Roque, A.C.A. Effects of phase transfer ligands on monodisperse iron oxide magnetic nanoparticles. *J. Coll. Interf. Sci.* **2015**, *437*, 147–155. [[CrossRef](#)]
52. Yoon, T.-J.; Lee, H.; Shao, H.; Hilderbrand, S.A.; Weissleder, R. Multicore Assemblies Potentiate Magnetic Properties of Biomagnetic Nanoparticles. *Adv. Mater.* **2011**, *23*, 4793–4797. [[CrossRef](#)] [[PubMed](#)]
53. Dutz, S.; Kettering, M.; Hilger, I.; Müller, R.; Zeisberger, M. Magnetic multicore nanoparticles for hyperthermia—Influence of particle immobilization in tumour tissue on magnetic properties. *Nanotechnology* **2011**, *22*, 265102. [[CrossRef](#)] [[PubMed](#)]
54. Dennis, C.L.; Krycka, K.L.; Borchers, J.A.; Desautels, R.D.; van Lierop, J.; Huls, N.F.; Jackson, A.J.; Gruettner, C.; Ivkov, R. Internal magnetic structure of nanoparticles dominates time-dependent relaxation processes in a magnetic field. *Adv. Funct. Mater.* **2015**, *25*, 4300–4311. [[CrossRef](#)]
55. Lee, H.; Shin, T.-H.; Cheon, J.; Weissleder, R. Recent Developments in Magnetic Diagnostic Systems. *Chem. Rev.* **2015**, *115*, 10690–10724. [[CrossRef](#)]
56. Ahrentorp, F.; Blomgren, J.; Jonasson, C.; Sarwe, A.; Sepehri, S.; Eriksson, E.; Kalaboukhov, A.; Jesorka, A.; Winkler, D.; Schneiderman, J.; et al. Sensitive magnetic biodetection using magnetic multi-core nanoparticles and RCA coils. *J. Magn. Magn. Mater.* **2017**, *427*, 14–18. [[CrossRef](#)]
57. Timko, M.; Molcan, M.; Hashim, A.; Skumiel, A.; Muller, M.; Gojzewski, H.; Jozefczak, A.; Kovac, J.; Rajnak, M.; Makowski, M.; et al. Hyperthermic effect in suspension of magnetosomes prepared by various methods. *IEEE Trans. Magn.* **2013**, *49*, 250–254. [[CrossRef](#)]
58. Baumgartner, J.; Bertinetti, L.; Widdrat, M.; Hirt, A.M.; Faivre, D. Formation of Magnetite Nanoparticles at Low Temperature: From Superparamagnetic to Stable Single Domain Particles. *PLoS ONE* **2013**, *8*, e57070. [[CrossRef](#)]
59. Bigall, N.C.; Wilhelm, C.; Beoutis, M.-L.; García-Hernandez, M.; Khan, A.A.; Giannini, C.; Sánchez-Ferrer, A.; Mezzenga, R.; Matera, M.E.; Garcia, M.A.; et al. Colloidal ordered assemblies in a polymer shell—A novel type of magnetic nanobeads for theranostic applications. *Chem. Mater.* **2013**, *25*, 1055–1062. [[CrossRef](#)]
60. Landfester, K. Synthesis of Colloidal Particles in Miniemulsions. *Annu. Rev. Mater. Res.* **2006**, *36*, 231–279. [[CrossRef](#)]
61. Qiu, P.; Jensen, C.; Charity, N.; Towner, R.; Mao, C. Oil phase evaporation-induced self-assembly of hydrophobic nanoparticles into spherical clusters with controlled surface chemistry in an oil-in-water dispersion and comparison of behaviors of individual and clustered iron oxide nanoparticles. *J. Am. Chem. Soc.* **2010**, *132*, 17724–17732. [[CrossRef](#)]
62. Paquet, C.; de Haan, H.W.; Leek, D.M.; Lin, H.-Y.; Xiang, B.; Tian, G.; Kell, A.; Simard, B. Clusters of superparamagnetic iron oxide nanoparticles encapsulated in a hydrogel: A particle architecture generating a synergistic enhancement of the T2 relaxation. *ACS Nano* **2011**, *5*, 3104–3112. [[CrossRef](#)]
63. Turcu, R.; Socoliuc, V.; Craciunescu, I.; Petran, A.; Paulus, A.; Franzreb, M.; Vasile, E.; Vekas, L. Magnetic microgels, a promising candidate for enhanced magnetic adsorbent particles in bioseparation: Synthesis, physicochemical characterization, and separation performance. *Soft Matter* **2015**, *11*, 1008–1018. [[CrossRef](#)] [[PubMed](#)]
64. Turcu, R.; Craciunescu, I.; Garamus, V.M.; Janko, C.; Lye, S.R.; Tietze, R.; Alexiou, C.; Vékás, L. Magnetic microgels for drug targeting applications: Physical–chemical properties and cytotoxicity evaluation. *J. Magn. Magn. Mater.* **2015**, *380*, 307–314. [[CrossRef](#)]
65. Hobson, N.J.; Weng, X.; Siow, B.; Veiga, C.; Ashford, M.; Thanh, N.T.K.; Schatzlein, A.G.; Uchegbu, I.F. Clustering superparamagnetic iron oxide nanoparticles produces organ-targeted high-contrast magnetic resonance images. *Nanomedicine* **2019**, *14*, 1135–1152. [[CrossRef](#)] [[PubMed](#)]
66. Peddis, D.; Cannas, C.; Musinu, A.; Ardu, A.; Orrù, F.; Fiorani, D.; Laureti, S.; Rinaldi, D.; Muscas, G.; Concas, G.; et al. Beyond the Effect of Particle Size: Influence of CoFe₂O₄ Nanoparticle Arrangements on Magnetic Properties. *Chem. Mater.* **2013**, *25*, 2005–2013. [[CrossRef](#)]

67. Vangijzegem, T.; Stanicki, D.; Laurent, S. Magnetic iron oxide nanoparticles for drug delivery: Applications and characteristics. *Expert Opin. Drug Deliv.* **2019**, *16*, 69–78. [[CrossRef](#)]
68. Laurent, S.; Saei, A.A.; Behzadi, S.; Panahifar, A.; Mahmoudi, M. Superparamagnetic iron oxide nanoparticles for delivery of therapeutic agents: Opportunities and challenges. *Expert Opin. Drug Deliv.* **2014**, *11*, 1–22. [[CrossRef](#)]
69. Qu, H.; Tong, S.; Song, K.; Ma, H.; Bao, G.; Pincus, S.; Zhou, W.; O'Connor, C. Controllable in situ synthesis of magnetite coated silica-core water-dispersible hybrid nanomaterials. *Langmuir* **2013**, *29*, 10573–10578. [[CrossRef](#)]
70. Szabo, T.; Bakandritsos, A.; Tzitzios, V.; Papp, S.; Korosi, L.; Galbacs, G.; Musabekov, K.; Bolatova, D.; Petridis, D.; Dekany, I. Magnetic iron oxide/clay composites: Effect of the layer silicate support on the microstructure and phase formation of magnetic nanoparticles. *Nanotechnology* **2007**, *18*, 285602. [[CrossRef](#)]
71. Amstad, E.; Textor, M.; Reimhult, E. Stabilization and functionalization of iron oxide nanoparticles for biomedical applications. *Nanoscale* **2011**, *3*, 2819–2843. [[CrossRef](#)]
72. Laurenti, M.; Guardia, P.; Contreras-Cáceres, R.; Pérez-Juste, J.; Fernandez-Barbero, A.; Lopez-Cabarcos, E.; Rubio-Retama, J. Synthesis of thermosensitive microgels with a tunable magnetic core. *Langmuir* **2011**, *27*, 10484–10491. [[CrossRef](#)] [[PubMed](#)]
73. Béalle, G.; Di Corato, R.; Kolosnjaj-Tabi, J.; Dupuis, V.; Clément, O.; Gazeau, F.; Wilhelm, C.; Ménager, C. Ultra magnetic liposomes for MR imaging, targeting, and hyperthermia. *Langmuir* **2012**, *28*, 11834–11842. [[CrossRef](#)] [[PubMed](#)]
74. Namiki, Y.; Namiki, T.; Yoshida, H.; Ishii, Y.; Tsubota, A.; Koido, S.; Nariai, K.; Mitsunaga, M.; Yanagisawa, S.; Kashiwagi, H.; et al. A novel magnetic crystal-lipid nanostructure for magnetically guided in vivo gene delivery. *Nat. Nanotechnol.* **2009**, *4*, 598–606. [[CrossRef](#)] [[PubMed](#)]
75. Mikhaylov, G.; Mikac, U.; Magaeva, A.A.; Itin, V.I.; Naiden, E.P.; Psakhye, I.; Babes, L.; Reinheckel, T.; Peters, C.; Zeiser, R.; et al. Ferri-liposomes as an MRI-visible drug-delivery system for targeting tumours and their microenvironment. *Nat. Nanotechnol.* **2011**, *6*, 594–602. [[CrossRef](#)]
76. Kong, S.D.; Choi, C.; Khamwannah, J.; Jin, S. Magnetically Vectored Delivery of Cancer Drug Using Remotely On–Off Switchable NanoCapsules. *IEEE Trans. Magn.* **2013**, *49*, 349–352. [[CrossRef](#)]
77. Bleul, R.; Thiermann, R.; Marten, G.U.; House, M.J.; St Pierre, T.G.; Häfeli, U.O.; Maskos, M. Continuously manufactured magnetic polymersomes—A versatile tool (not only) for targeted cancer therapy. *Nanoscale* **2013**, *5*, 11385–11393. [[CrossRef](#)]
78. Bannwarth, M.B.; Utech, S.; Ebert, S.; Weitz, D.A.; Crespy, D.; Landfester, K. Colloidal Polymers with Controlled Sequence and Branching Constructed from Magnetic Field Assembled Nanoparticles. *ACS Nano* **2015**, *9*, 2720–2728. [[CrossRef](#)]
79. Hu, M.; Butt, H.-J.; Landfester, K.; Bannwarth, M.B.; Wooh, S.; Thérien-Aubin, H. Shaping the Assembly of Superparamagnetic Nanoparticles. *ACS Nano* **2019**, *13*, 3015–3022. [[CrossRef](#)]
80. Savva, I.; Odysseos, A.D.; Evaggelou, L.; Marinica, O.; Vasile, E.; Vekas, L.; Sarigiannis, Y.; Krasia-Christoforou, T. Fabrication, Characterization, and Evaluation in Drug Release Properties of Magnetoactive Poly(ethylene oxide)-Poly(L-lactide) Electrospun Membranes. *Biomacromolecules* **2013**, *14*, 4436–4446. [[CrossRef](#)]
81. Papaphilippou, P.; Christodoulou, M.; Marinica, O.; Taculescu, A.; Vekas, L.; Chrissafis, K.; Krasia-Christoforou, T. Multiresponsive Polymer Conetworks Capable of Responding to Changes in pH, Temperature, and Magnetic Field: Synthesis, Characterization, and Evaluation of Their Ability for Controlled Uptake and Release of Solutes. *ACS Appl. Mater. Interfaces* **2012**, *4*, 2139–2147. [[CrossRef](#)]
82. Gavilan, H.; Kowalski, A.; Heinke, D.; Sugunan, A.; Sommertune, J.; Varon, M.; Bogart, L.K.; Posth, O.; Zeng, L.; Gonzalez-Alonso, D.; et al. Colloidal Flower-Shaped Iron Oxide Nanoparticles: Synthesis Strategies and Coatings. *Part. Part. Syst. Charact.* **2017**, *34*, 1700094. [[CrossRef](#)]
83. Gutiérrez, L.; de la Cueva, L.; Moros, M.; Mazarío, E.; Bernardo, S.; de la Fuente, J.M.; Morales, M.P.; Salas, G. Aggregation effects on the magnetic properties of iron oxide colloids. *Nanotechnology* **2019**, *30*, 112001. [[CrossRef](#)] [[PubMed](#)]
84. Lartigue, L.; Hugounenq, P.; Alloyeau, D.; Clarke, S.P.; Lévy, M.; Bacri, J.-C.; Bazzi, R.; Brougham, D.F.; Wilhelm, C.; Gazeau, F. Cooperative organization in iron oxide multi-core nanoparticles potentiates their efficiency as heating mediators and MRI contrast agents. *ACS Nano* **2012**, *6*, 10935–10949. [[CrossRef](#)] [[PubMed](#)]

85. Vasilescu, C.; Latikka, M.; Knudsen, K.D.; Garamus, V.M.; Socoliuc, V.R.; Tombácz, E.; Susan-Resiga, D.; Ras, R.H.A.; Vékás, L. High concentration aqueous magnetic fluids: Structure, colloidal stability, magnetic and flow properties. *Soft Matter* **2018**, *14*, 6648. [\[CrossRef\]](#)
86. Tombácz, E.; Illés, E.; Majzik, A.; Hajdú, A. Ageing in the Inorganic Nanoworld: Example of Magnetite Nanoparticles in Aqueous Medium. *Croat. Chem. Acta* **2007**, *80*, 503–515.
87. Forge, D.; Laurent, S.; Gossuin, Y.; Roch, A.; Van der Elst, L.; Muller, R.N. An original route to stabilize and functionalize magnetite nanoparticles for theranosis applications. *J. Magn. Magn. Mater.* **2011**, *323*, 410–415. [\[CrossRef\]](#)
88. Ramimoghadam, D.; Bagheri, S.; Abd Hamid, S.B. Stable monodisperse nanomagnetic colloidal suspensions: An overview. *Colloids Surf. B Biointerfaces* **2015**, *133*, 388–411. [\[CrossRef\]](#)
89. Creixell, M.; Herrera, A.P.; Latorre-Esteves, M.; Ayala, V.; Torres-Lugo, M.; Rinaldi, C. The effect of grafting method on the colloidal stability and in vitro cytotoxicity of carboxymethyl dextran coated magnetic nanoparticles. *J. Mater. Chem.* **2010**, *20*, 8539–8547. [\[CrossRef\]](#)
90. Barrera, C.; Herrera, A.P.; Bezares, N.; Fachini, E.; Olayo-Valles, R.; Hinestroza, J.P.; Rinaldi, C. Effect of poly(ethylene oxide)-silane graft molecular weight on the colloidal properties of iron oxide nanoparticles for biomedical applications. *J. Colloid Interface Sci.* **2012**, *377*, 40–50. [\[CrossRef\]](#) [\[PubMed\]](#)
91. Mihai, M.; Socoliuc, V.; Doroftei, F.; Ursu, E.-L.; Aflori, M.; Vekas, L.; Simionescu, B.C. Calcium Carbonate–Magnetite–Chondroitin Sulfate Composite Microparticles with Enhanced pH Stability and Superparamagnetic Properties. *Cryst. Growth Des.* **2013**, *13*, 3535–3545. [\[CrossRef\]](#)
92. Bunia, I.; Socoliuc, V.; Vekas, L.; Doroftei, F.; Varganici, C.; Coroaba, A.; Simionescu, B.C.; Mihai, M. Superparamagnetic Composites Based on Ionic Resin Beads/CaCO₃/Magnetite. *Chem. A Eur. J.* **2016**, *22*, 18036–18044. [\[CrossRef\]](#) [\[PubMed\]](#)
93. Biliuta, G.; Secarescu, L.; Socoliuc, V.; Iacob, M.; Gheorghe, L.; Negru, D.; Coseri, S. Carboxylated Polysaccharides Decorated with Ultrasmall Magnetic Nanoparticles with Antibacterial and MRI Properties. *Macromol. Chem. Phys.* **2017**, *218*, 1700062. [\[CrossRef\]](#)
94. Tóth, I.Y.; Illés, E.; Szekeres, M.; Zupkó, I.; Turcu, R.; Tombácz, E. Chondroitin-Sulfate-A-Coated Magnetite Nanoparticles: Synthesis, Characterization and Testing to Predict Their Colloidal Behavior in Biological Milieu. *Int. J. Mol. Sci.* **2019**, *20*, 4096. [\[CrossRef\]](#) [\[PubMed\]](#)
95. Boyer, C.; Whittaker, M.R.; Bulmus, V.; Liu, J.; Davis, T.P. The design and utility of polymer-stabilized iron-oxide nanoparticles for nanomedicine applications. *NPG Asia Mater.* **2010**, *2*, 23–30. [\[CrossRef\]](#)
96. Kumar, C. *Magnetic Nanomaterials*; Wiley-VCH: Weinheim, Germany, 2009.
97. Blanco-Andujar, C.; Ortega, D.; Southern, P.; Pankhurst, Q.A.; Thanh, N.T.K. High performance multi-core iron oxide nanoparticles for magnetic hyperthermia: Microwave synthesis, and the role of core-to-core interactions. *Nanoscale* **2015**, *7*, 1768–1775. [\[CrossRef\]](#) [\[PubMed\]](#)
98. Szekeres, M.; Tóth, I.Y.; Illés, E.; Hajdú, A.; Zupkó, I.; Farkas, K.; Oszlanczi, G.; Tiszlavicz, L.; Tombácz, E. Chemical and colloidal stability of carboxylated core-shell magnetite nanoparticles designed for biomedical applications. *Int. J. Mol. Sci.* **2013**, *14*, 14550–14574. [\[CrossRef\]](#)
99. Jedlovsky-Hajdú, A.; Bombelli, F.B.; Monopoli, M.P.; Tombácz, E.; Dawson, K.A. Surface coatings shape the protein corona of SPIONs with relevance to their application in vivo. *Langmuir* **2012**, *28*, 14983–14991. [\[CrossRef\]](#) [\[PubMed\]](#)
100. Lartigue, L.; Innocenti, C.; Kalaivani, T.; Awwad, A.; Mar Sanchez Duque, M.; Guari, Y.; Larionova, J.; Guerin, C.; Montero, J.G.; Barragan-Montero, V.; et al. Water-Dispersible Sugar-Coated Iron Oxide Nanoparticles. An Evaluation of their Relaxometric and Magnetic Hyperthermia Properties. *J. Am. Chem. Soc.* **2011**, *133*, 10459–10472. [\[CrossRef\]](#)
101. Weidner, A.; Gräfe, C.; von der Lühe, M.; Remmer, H.; Clement, J.H.; Eberbeck, D.; Ludwig, F.; Müller, R.; Schacher, F.H.; Dutz, S. Preparation of Core-Shell Hybrid Materials by Producing a Protein Corona Around Magnetic Nanoparticles. *Nanoscale Res. Lett.* **2015**, *10*, 282. [\[CrossRef\]](#)
102. Wang, J.; Zhang, B.; Wang, L.; Wang, M.; Gao, F. One-pot synthesis of water-soluble superparamagnetic iron oxide nanoparticles and their MRI contrast effects in the mouse brains. *Mater. Sci. Eng. C* **2015**, *48*, 416–423. [\[CrossRef\]](#)
103. Illés, E.; Szekeres, M.; Tóth, I.Y.; Szabó, Á.; Iván, B.; Turcu, R.; Vékás, L.; Zupkó, I.; Jaics, G.; Tombácz, E. Multifunctional PEG-carboxylate copolymer coated superparamagnetic iron oxide nanoparticles for biomedical application. *J. Magn. Magn. Mater.* **2018**, *451*, 710–720. [\[CrossRef\]](#)

104. Socoliuc, V.-M.; Vékás, L. Hydrophobic and hydrophilic magnetite nanoparticles: Synthesis by chemical coprecipitation and physico-chemical characterization. In *Upscaling of Bio-Nano-Processes*; Nirschl, H., Keller, K., Eds.; Springer: Berlin, Germany, 2014; pp. 39–55.
105. Zaloga, J.; Janko, C.; Nowak, J.; Matuszak, J.; Knaup, S.; Eberbeck, D.; Tietze, R.; Unterweger, H.; Friedrich, R.P.; Duerr, S.; et al. Development of a lauric acid/albumin hybrid iron oxide nanoparticle system with improved biocompatibility. *Int. J. Nanomed.* **2014**, *9*, 4847–4866. [[CrossRef](#)] [[PubMed](#)]
106. Abakumov, M.A.; Nukolova, N.V.; Sokolsky-Papkov, M.; Shein, S.A.; Sandalova, T.O.; Vishwasrao, H.M.; Grinenko, N.F.; Gubsky, I.L.; Abakumov, A.M.; Kabanov, A.V.; et al. VEGF-targeted magnetic nanoparticles for MRI visualization of brain tumor. *Nanomedicine Nanotechnology. Biol. Med.* **2015**, *11*, 825–833.
107. Nel, A.E.; Mädler, L.; Velegol, D.; Xia, T.; Hoek, E.M.V.; Somasundaran, P.; Klaessig, F.; Castranova, V.; Thompson, M. Understanding biophysicochemical interactions at the nano-bio interface. *Nat. Mater.* **2009**, *8*, 8543–8557. [[CrossRef](#)] [[PubMed](#)]
108. Tombacz, E.; Farkas, K.; Foldesi, I.; Szekeres, M.; Illes, E.; Toth, I.Y.; Nesztor, D.; Szabo, T. Polyelectrolyte coating on superparamagnetic iron oxide nanoparticles as interface between magnetic core and biorelevant media. *Interface Focus* **2016**, *6*, 20160068. [[CrossRef](#)] [[PubMed](#)]
109. EMA. EMA/325027/2013. *Reflection Paper on Surface Coatings: General Issues for Consideration Regarding Parenteral Administration of Coated Nanomedicine Products*; European Medicines Agency: Amsterdam, The Netherlands, 22 May 2013. Available online: https://www.ema.europa.eu/en/documents/scientific-guideline/reflection-paper-surface-coatings-general-issues-consideration-regarding-parenteral-administration_en.pdf (accessed on 19 December 2019).
110. Elimelech, M.; Gregory, J.; Jia, X.; Williams, R. *Particle Deposition and Aggregation, Measurement, Modelling and Simulation*; Butterworth-Heinemann Ltd.: Oxford, UK, 1995.
111. Gregory, J. *Particles in Water, Properties and Processes*; CRC Press Taylor & Francis Group: Boca Raton, FL, USA, 2006.
112. Eberbeck, D.; Wiekhorst, F.; Steinhoff, U.; Trahms, L. Aggregation behaviour of magnetic nanoparticle suspensions investigated by magnetorelaxometry. *J. Phys. Condens. Matter.* **2006**, *18*, 2829–2846. [[CrossRef](#)]
113. Nel, A.E.; Brinker, C.J.; Parak, W.J.; Zink, J.I.; Chan, W.C.W.; Pinkerton, K.E.; Xia, T.; Baer, D.R.; Hersam, M.C.; Weiss, P.S. Where Are We Heading in Nanotechnology Environmental Health and Safety and Materials Characterization? *ACS Nano* **2015**, *9*, 5627–5630. [[CrossRef](#)]
114. Kolen'ko, Y.V.; Bañobre-López, M.; Rodríguez-Abreu, C.; Carbó-Argibay, E.; Sailsman, A.; Piñeiro-Redondo, Y.; Fátima Cerqueira, M.; Petrovykh, D.Y.; Kovnir, K.; Lebedev, O.I.; et al. Large-Scale Synthesis of Colloidal Fe₃O₄ Nanoparticles Exhibiting High Heating Efficiency in Magnetic Hyperthermia. *J. Phys. Chem. C* **2014**, *118*, 8691–8701. [[CrossRef](#)]
115. Di Corato, R.; Aloisi, A.; Rella, S.; Greneche, J.M.; Pugliese, G.; Pellegrino, T.; Malitesta, C.; Rinaldi, R. Maghemite Nanoparticles with Enhanced Magnetic Properties: One-Pot Preparation and Ultrastable Dextran Shell. *ACS Appl. Mater. Interfaces* **2018**, *10*, 20271–20280. [[CrossRef](#)]
116. Tóth, Y.I.; Szekeres, M.; Turcu, R.; Sáring, S.; Illes, E.; Nesztor, D.; Tombácz, E. Mechanism of in Situ Surface Polymerization of Gallic Acid in an Environmental-Inspired Preparation of Carboxylated Core-Shell Magnetite Nanoparticles. *Langmuir* **2014**, *30*, 15451–15461. [[CrossRef](#)]
117. Nan, A.; Radu, T.; Turcu, R. Poly(glycidyl methacrylate)-functionalized magnetic nanoparticles as platforms for linking functionalities, bioentities and organocatalysts. *RSC Adv.* **2016**, *6*, 43330–43338. [[CrossRef](#)]
118. Willis, A.L.; Turro, N.J.; O'Brien, S. Spectroscopic Characterization of the Surface of Iron Oxide Nanocrystals. *Chem. Mater.* **2005**, *17*, 5970–5975. [[CrossRef](#)]
119. Daou, T.J.; Pourroy, G.; Begin-Colin, S.; Greneche, J.M.; Ulhaq-Bouillet, C.; Legare, P.; Bernhardt, P.; Leuvrey, C.; Rogez, G. Hydrothermal synthesis of monodisperse magnetite nanoparticles. *Chem. Mater.* **2006**, *18*, 4399–4404. [[CrossRef](#)]
120. Wilson, D.; Langell, M.A. XPS analysis of oleylamine/oleic acid capped Fe₃O₄ nanoparticles as a function of temperature. *Appl. Surf. Sci.* **2014**, *303*, 6–13. [[CrossRef](#)]
121. Roth, H.-C.; Schwaminger, S.P.; Schindler, M.; Wagner, F.E.; Berensmeier, S. Influencing factors in the CO-precipitation process of superparamagnetic iron oxide nanoparticles: A model based study. *J. Magn. Magn. Mater.* **2015**, *377*, 81–89. [[CrossRef](#)]

122. Daou, T.J.; Begin-Colin, S.; Greneche, J.M.; Thomas, F.; Derory, A.; Bernhardt, P.; Legare, P.; Pourroy, G. Phosphate Adsorption Properties of Magnetite-Based Nanoparticles. *Chem. Mater.* **2007**, *19*, 4494–4505. [[CrossRef](#)]
123. Walter, A.; Garofalo, A.; Parat, A.; Martinez, H.; Felder-Flesch, D.; Begin-Colin, S. Functionalization strategies and dendronization of iron oxide nanoparticles. *Nanotechnol. Rev.* **2015**, *4*, 581–593. [[CrossRef](#)]
124. Palanisamy, S.; Wang, Y.-M. Superparamagnetic Iron oxide Nanoparticulate System: Synthesis, Targeting, Drug Delivery and Therapy in Cancer. *Dalton Trans.* **2019**, *48*, 9490–9515. [[CrossRef](#)]
125. Mazur, M.; Barras, A.; Kuncser, V.; Galatanu, A.; Zaitzev, V.; Turcheniuk, K.V.; Woisel, P.; Lyskawa, J.; Laure, W.; Siriwardena, A.; et al. Iron oxide magnetic nanoparticles with versatile surface functions based on dopamine anchors. *Nanoscale* **2013**, *5*, 2692–2702. [[CrossRef](#)]
126. Safi, M.; Courtois, J.; Seigneuret, M.; Conjeaud, H.; Berret, J.-F. The effects of aggregation and protein corona on the cellular internalization of iron oxide nanoparticles. *Biomaterials* **2011**, *32*, 9353–9363. [[CrossRef](#)]
127. Calatayud, M.P.; Sanz, B.; Raffa, V.; Riggio, C.; Ibarra, M.R.; Goya, G.F. The effect of surface charge of functionalized Fe₃O₄ nanoparticles on protein adsorption and cell uptake. *Biomaterials* **2014**, *35*, 6389–6399. [[CrossRef](#)] [[PubMed](#)]
128. Szekeres, M.; Tóth, I.Y.; Turcu, R.; Tombácz, E. The effect of polycarboxylate shell of magnetite nanoparticles on protein corona formation in blood plasma. *J. Magn. Magn. Mater.* **2017**, *427*, 95–99. [[CrossRef](#)]
129. Dürr, S.; Janko, C.; Lyer, S.; Tripal, P.; Schwarz, M.; Jan, Z.; Tietze, R.; Alexiou, C. Magnetic Nanoparticles for Cancer Therapy. *Nanotechnol. Rev.* **2013**, *2*, 395–409. [[CrossRef](#)]
130. Pinho, S.L.C.; Pereira, G.A.; Voisin, P.; Kassem, J.; Bouchaud, V.; Etienne, L.; Peters, J.A.; Carlos, L.; Mornet, S.; Geraldès, C.F.G.C.; et al. Fine Tuning of the Relaxometry of gamma-Fe₂O₃@SiO₂ Nanoparticles by Tweaking the Silica Coating Thickness. *ACS Nano* **2010**, *4*, 5339–5349. [[CrossRef](#)] [[PubMed](#)]
131. Tombácz, E.; Szekeres, M.; Hajdú, A.; Tóth, I.Y.; Bauer, R.A.; Nesztor, D.; Illés, E.; Zupkó, I.; Vékás, L. Colloidal stability of carboxylated iron oxide nanomagnets for biomedical use. *Period. Polytech. Chem. Eng.* **2014**, *58*, 3–10. [[CrossRef](#)]
132. Toth, I.Y.; Illes, E.; Bauer, R.A.; Nesztor, D.; Szekeres, M.; Zupko, I.; Tombacz, E. Designed polyelectrolyte shell on magnetite nanocore for dilution-resistant biocompatible magnetic fluids. *Langmuir* **2012**, *28*, 16638–16646. [[CrossRef](#)]
133. Socoliuc, V.; Turcu, R.; Kuncser, V.; Vekas, L. Magnetic Characterization. In *Contrast Agents for MRI-Experimental Methods*; Pierre, V.C., Allen, M.J., Eds.; Royal Society of Chemistry: Brighton, UK, 2018; pp. 391–426.
134. Garaio, E.; Collantes, J.M.; Plazaola, F.; Garcia, J.A.; Castellanos-Rubio, I. A multifrequency electromagnetic applicator with an integrated AC magnetometer for magnetic hyperthermia experiments. *Meas. Sci. Technol.* **2014**, *25*, 115702. [[CrossRef](#)]
135. Lenox, P.; Plummer, L.K.; Paul, P.; Hutchison, J.E.; Jander, A.; Dhagat, P. High-Frequency and High-Field Hysteresis Loop Tracer for Magnetic Nanoparticle Characterization. *IEEE Magn. Lett.* **2018**, *9*, 6500405. [[CrossRef](#)]
136. Fannin, P.; Marin, C.N.; Malaescu, I.; Raj, K.; Popoiu, C. Local arrangement of particles in magnetic fluids due to the measurement alternating field. *J. Magn. Magn. Mater.* **2017**, *438*, 116–120. [[CrossRef](#)]
137. Pedersen, J.S. Analysis of small-angle scattering data from colloids and polymer solutions: Modeling and least-squares fitting. *Adv. Colloid Interface Sci.* **1997**, *70*, 171–210. [[CrossRef](#)]
138. Mühlbauer, S.; Honecker, D.; Périgo, É.A.; Bergner, F.; Disch, S.; Heinemann, A.; Erokhin, S.; Berkov, D.; Leighton, C.; Ring Eskildsen, M.; et al. Magnetic small-angle neutron scattering. *Rev. Mod. Phys.* **2019**, *91*, 015004. [[CrossRef](#)]
139. Avdeev, M.V.; Aksenov, V.L. Small-angle neutron scattering in structure research of magnetic fluids. *Phys. Usp.* **2010**, *53*, 971–993. [[CrossRef](#)]
140. Avdeev, M.V.; Petrenko, V.I.; Gapon, I.V.; Bulavin, L.A.; Vorobiev, A.A.; Soltwedel, O.; Balasoiu, M.; Vekas, L.; Zavisova, V.; Kopcansky, P. Comparative structure analysis of magnetic fluids at interface with silicon by neutron reflectometry. *Appl. Surf. Sci.* **2015**, *352*, 49–53. [[CrossRef](#)]
141. Daillant, J.; Gibaud, A. (Eds.) *X-Ray and Neutron Reflectivity: Principles and Applications*; Springer: Berlin/Heidelberg, Germany, 2009.
142. Vorobiev, A.; Major, J.; Dosch, H.; Gordeev, G.; Orlova, D. Magnetic field dependent ordering in ferrofluids at SiO₂ interfaces. *Phys. Rev. Lett.* **2004**, *93*, 267203. [[CrossRef](#)] [[PubMed](#)]

143. Nagorny, A.V.; Petrenko, V.I.; Avdeev, M.V.; Yelenich, O.V.; Solopan, S.O.; Belous, A.G.; Gruzinov, A.Y.; Ivankov, O.I.; Bulavin, L.A. Structural aspects of magnetic fluid stabilization in aqueous agarose solutions. *J. Magn. Magn. Mater.* **2017**, *431*, 16–19. [[CrossRef](#)]
144. Petrenko, V.I.; Aksenov, V.L.; Avdeev, M.V.; Bulavin, L.A.; Rosta, L.; Vekas, L.; Garamus, V.M.; Willumeit, R. Analysis of the structure of aqueous ferrofluids by the small-angle neutron scattering method. *Phys. Solid State* **2010**, *52*, 974–978. [[CrossRef](#)]
145. Avdeev, M.V.; Feoktystov, A.V.; Kopcansky, P.; Lancz, G.; Garamus, V.M.; Willumeit, R.; Jurikova, A.J.; Timiko, M.; Zavisova, V.; Csach, K.; et al. Structure of water-based ferrofluids with sodium oleate and polyethylene glycol stabilization by small-angle neutron scattering: contrast-variation experiments. *J. Appl. Cryst.* **2010**, *43*, 959–969. [[CrossRef](#)]
146. Petrenko, V.I.; Artykulnyi, O.P.; Bulavin, L.A.; Almásy, L.; Garamus, V.M.; Ivankov, O.I.; Grigoryeva, N.A.; Vekas, L.; Kopcansky, P.; Avdeev, M.V. On the impact of surfactant type on the structure of aqueous ferrofluids. *Colloids Surf. A* **2018**, *541*, 222–226. [[CrossRef](#)]
147. Petrenko, V.I.; Avdeev, M.V.; Garamus, V.M.; Bulavin, L.A.; Kopcansky, P. Impact of polyethylene glycol on aqueous micellar solutions of sodium oleate studied by small-angle neutron scattering. *Colloids Surf. A* **2015**, *480*, 191–196. [[CrossRef](#)]
148. Lancz, G.; Avdeev, M.V.; Petrenko, V.I.; Garamus, V.M.; Koneracká, M.; Kopčanský, P. SANS study of poly(ethylene glycol) solutions in D₂O. *Acta Phys. Polonica A* **2010**, *118*, 980–982. [[CrossRef](#)]
149. Artykulnyi, O.P.; Petrenko, V.I.; Bulavin, L.A.; Ivankov, O.I.; Avdeev, M.V. Impact of poly(ethylene glycol) on the structure and interaction parameters of aqueous micellar solutions of anionic surfactants. *J. Mol. Liq.* **2019**, *276*, 806–811. [[CrossRef](#)]
150. Melníková, L.; Petrenko, V.I.; Avdeev, M.V.; Garamus, V.M.; Almásy, L.; Ivankov, O.I.; Bulavin, L.A.; Mitróová, Z.; Kopcansky, P. Effect of iron oxide loading on magnetoferritin structure in solution as revealed by SAXS and SANS. *Colloids Surf. B* **2014**, *123*, 82–88.
151. Majorosova, J.; Petrenko, V.I.; Siposova, K.; Timko, M.; Tomasovicova, N.; Garamus, V.M.; Koralewski, M.; Avdeev, M.V.; Leszczynski, B.; Jurga, S.; et al. On the adsorption of magnetite nanoparticles on lysozyme amyloid fibrils. *Colloids Surf. B* **2016**, *146*, 794–800. [[CrossRef](#)] [[PubMed](#)]
152. Petrenko, V.I.; Nagorny, A.V.; Gapon, I.V.; Vekas, L.; Garamus, V.M.; Almasy, L.; Feoktystov, A.V.; Avdeev, M.V. Magnetic Fluids: Structural Aspects by Scattering Techniques. In *Modern Problems of Molecular Physics*; Bulavin, L., Chalyi, A., Eds.; Springer: Cham, Switzerland, 2018; Volume 197, pp. 205–226.
153. Kubovcikova, M.; Gapon, I.V.; Zavisova, V.; Koneracka, M.; Petrenko, V.I.; Soltwedel, O.; Almasy, L.; Avdeev, M.V.; Kopcansky, P. On the adsorption properties of magnetic fluids: Impact of bulk structure. *J. Magn. Magn. Mater.* **2017**, *427*, 67–70. [[CrossRef](#)]
154. Avdeev, M.V.; Petrenko, V.I.; Feoktystov, A.V.; Gapon, I.V.; Aksenov, V.L.; Vekás, L.; Kopčanský, P. Neutron investigations of ferrofluids. *Ukr. J. Phys.* **2015**, *60*, 728–736. [[CrossRef](#)]
155. Theis-Bröhl, K.; Gutfreund, P.; Vorobiev, A.; Wolff, M.; Toperverg, B.P.; Dura, J.A.; Borchers, J.A. Self assembly of magnetic nanoparticles at silicon surfaces. *Soft Matter* **2015**, *11*, 4695–4704. [[CrossRef](#)] [[PubMed](#)]
156. Theis-Bröhl, K.; Vreeland, E.C.; Gomez, A.; Huber, D.L.; Saini, A.; Wolff, M.; Maranville, B.B.; Brok, E.; Krycka, K.L.; Dura, J.A.; et al. Self-assembled layering of magnetic nanoparticles in a ferrofluid on silicon surfaces. *ACS Appl. Mater. Interfaces* **2018**, *10*, 5050–5060.
157. Berne, B.J.; Pecora, R. *Dynamic Light Scattering*; John Wiley: New York, NY, USA, 1976.
158. Bohren, C.F.; Huffman, D.R. *Absorption and Scattering of Light by Small Particles*; Wiley-Interscience: New York, NY, USA, 2010.
159. Socoliuc, V.; Turcu, R. Large scale aggregation in magnetic colloids induced by high frequency magnetic fields. *J. Magn. Magn. Mater.* **2019**, accepted. [[CrossRef](#)]
160. Dennis, C.L.; Jackson, A.J.; Borchers, J.A.; Gruettner, C.; Ivkov, R. Correlation between physical structure and magnetic anisotropy of a magnetic nanoparticle colloid. *Nanotechnology* **2018**, *29*, 215705. [[CrossRef](#)]
161. Massart, R. *Magnetic Fluids and Applications Handbook*; Berkovski, B.M., Bashtovoy, V.G., Eds.; Begell House: Washington, DC, USA, 1996; pp. 24–27.
162. Odenbach, S. Ferrofluids. In *Handbook of Magnetic Materials*; Buschow, K.H.J., Ed.; Elsevier Science: Amsterdam, The Netherlands, 2006; Volume 16, pp. 127–208.

163. Roger, S.; Sang, Y.Y.C.; Bee, A.; Perzynski, R.; Di Meglio, J.M.; Ponton, A. Structural and multi-scale rheophysical investigation of diphasic magneto-sensitive materials based on biopolymers. *Eur. Phys. J. E Soft Matter Biol. Phys.* **2015**, *38*, 88. [[CrossRef](#)]
164. Nowak, J.; Wiekhorst, F.; Trahms, L.; Odenbach, S. The influence of hydrodynamic diameter and core composition on the magnetoviscous effect of biocompatible ferrofluids. *J. Phys. Condens. Matter* **2014**, *26*, 176004. [[CrossRef](#)]
165. Dutz, S.; Clement, J.H.; Eberbeck, D.; Gelbrich, T.; Hergt, R.; Müller, R.; Wotschadlo, J.; Zeisberger, M. Ferrofluids of magnetic multicore nanoparticles for biomedical applications. *J. Magn. Magn. Mater.* **2009**, *321*, 1501–1504. [[CrossRef](#)]
166. Bender, P.; Bogart, L.K.; Posth, O.; Szczerba, W.; Rogers, S.E.; Castro, A.; Nilsson, L.; Zeng, L.J.; Sugunan, A.; Sommertune, J.; et al. Structural and magnetic properties of multi-core nanoparticles analysed using a generalized numerical inversion method. *Sci. Rep.* **2017**, *7*, 45990. [[CrossRef](#)]
167. Nowak, J.; Odenbach, S. A capillary viscometer designed for the characterization of biocompatible ferrofluids. *J. Magn. Magn. Mater.* **2016**, *411*, 49–54. [[CrossRef](#)]
168. Nowak, J.; Odenbach, S. Magnetoviscous effect in a biocompatible ferrofluid. *IEEE Trans. Magn.* **2013**, *49*, 208–212. [[CrossRef](#)]
169. Bossis, G.; Volkova, O.; Laci, S.; Meunier, A. Magnetorheology: Fluids, structures and rheology. In *Ferrofluids*; Springer: Berlin/Heidelberg, Germany, 2002; Volume 594, pp. 202–230.



© 2020 by the authors. Licensee MDPI, Basel, Switzerland. This article is an open access article distributed under the terms and conditions of the Creative Commons Attribution (CC BY) license (<http://creativecommons.org/licenses/by/4.0/>).